1. MAGNETIC CONFINEMENT

1. Magnetic

The Frascati Tokamak Upgrade (FTU) is a compact, high-magnetic-field tokamak capable of operating at density and magnetic field values similar to - or even encompassing - those of the International Thermonuclear Experimental Reactor (ITER) and therefore provides a unique opportunity to explore physics issues that are directly relevant to ITER.

During 2004 the experimental activities were focussed on fully exploiting the lower hybrid system (for generating and controlling the plasma current) and the electron cyclotron heating system (joint experiment with the Institute of Plasma Physics of the National Research Council, Milan). With all four gyrotrons in operation, full electron cyclotron power was achieved up to a record level of 1.5 MW. By simultaneously injecting lower hybrid waves, to tailor the plasma current radial profile, and electron cyclotron waves, to heat the plasma centre, good confinement regimes with internal transport barriers were obtained at the highest plasma density values ever achieved for this operation regime ($n \approx 1.5 \times 10^{20} m^{-3}$). Specific studies were devoted to optimising the coupling of lower hybrid waves to the plasma (by real-time control of the plasma position) and to generating current by electron cyclotron current drive.

The new scanning CO_2 interferometer (developed by the Reversed Field Experiment Consortium) for high spatial and time resolution (1 cm/50 μs) density profile measurements was extensively used. The Thomson scattering diagnostic was upgraded and enabled observation of scattered signals associated with the

Confinement

background plasma dynamics.

As for theoretical studies on the dynamics of turbulence in plasmas, the transition from Bohm-like scaling to gyro-Bohm scaling of the local plasma diffusivity was demonstrated on the basis of a generalised four-wave model (joint collaboration with Princeton Plasma Physics Laboratory and the University of California at Irvine). The transition from weak to strong energetic particle transport above a certain threshold in the energetic particle density in burning plasmas was further investigated by means of the hybrid magnetohydrodynamic gyro-kinetic code developed at Frascati.

The efforts devoted to the Joint European Torus (JET) campaign were limited to the first part of the year because the machine was in shutdown for most of 2004. ENEA was responsible for the coordination of Task Force S2 until the end of 2004 and was also in charge of the development of advanced scenarios for ITER. Further progress was achieved in developing real-time control tools (the extreme shape controller developed in collaboration with the CREATE Consortium [Universities of Naples, Cassino and Reggio Calabria] and advanced modes of operation with dominant electron heating (ENEA/Commissariat à l'Energie Atomique collaboration involving joint experimental activities on FTU, Tore Supra and JET). Important results were obtained in exploiting gamma-ray spectroscopy for the measurement of fast-ion distribution.

1.2.1 FTU machine

Summary of machine operation. During 2004 the machine operated at the same high level (about 90% of successful pulses) as it did in 2003.

Experimental activities started at the beginning of February, but had to be stopped after two weeks because of a leak in the scattering window. As a consequence, the vacuum vessel had to be vented and the conditioning procedures restarted. After three experimental days, activities were halted again in order to install the CO_2 interferometer.

Following the summer break, a two-month experimental campaign was devoted to achieving long-duration electron transport barriers. The lower hybrid (LH) and electron cyclotron resonance (ECR) systems were used simultaneously to heat the plasma and drive the current. The programme was successful.

Work on the control and data acquisition system included:

- Implementation of a new module in the plasma position control system in order to minimise the radiofrequency-lower hybrid power reflected by the FTU plasma.
- Completion and testing of a tool to simulate and generate new control modules by means of the Simulink tool box of the Matlab application.
- Design and first implementation of a general restyling of the FTU plasma density and position control system.
- Implementation of a three-node Andrew file system (AFS) cell by means of OpenSource software only: this could be a first approach to study OpenSource systems for ITER and/or IGNITOR.
- Upgrading of the FTU archive from 1 to 3 TeraBytes by means of a new disk system in order to meet the growing physics requests.
- Completion and testing of a Video Conference Server (Virtual Room Videoconferencing System [VRVS] reflector) to allow participation in seminars or meetings from a desktop personal computer (PC), without firewall restrictions.

During the reporting year, 1936 shots were successfully completed out of a total of 2172 performed over 89 experimental days. The average number of successful daily pulses was 21.75. Table 1.I reports the main parameters used for evaluating the efficiency of the experimental sessions. The main source of downtime, with a 26.5% share (fig. 1.1), was the time required to analyse experimental data. The indicator trend (fig. 1.2) shows that the experimental days picked up slightly compared to 2003. The experimental time indicator again shows a small decrease due, this time, to an increase in analysis time.

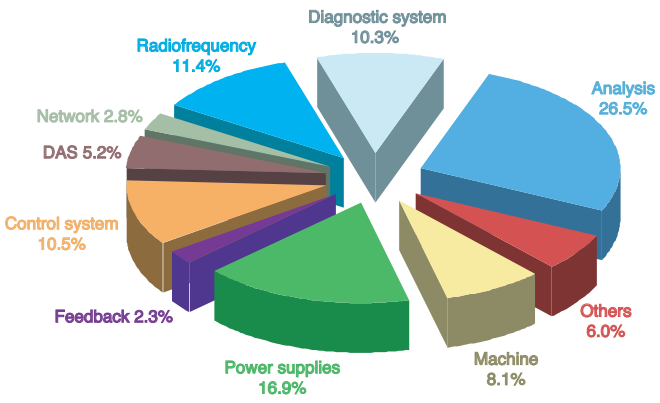

Fig. 1.1 - Downtime sources in 2004

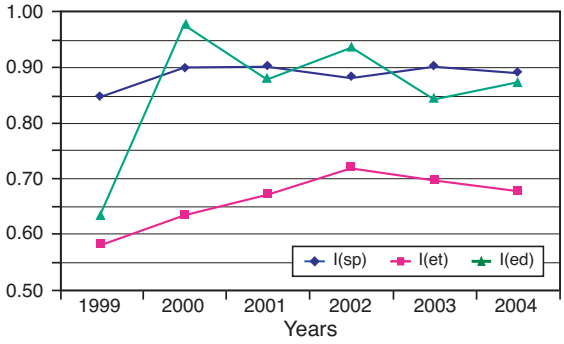

Fig. 1.2 - Indicator trend 1999 – 2004. I(sp): successful/total pulses. I(et): real/total experimental days. I(ed): real/total experimental time

1. Magnetic Confinement

Table 1.I – Summary of FTU operations in 2004

	Jan.	Feb.	March	April	May	June	July	Aug.	Sept.	Oct.	Nov.	Dec.	Total
Total pulses	0	184	220	262	358	310	0	15	375	448	0	0	2172
Successful pulses (sp)	0	151	205	247	312	282	0	13	325	401	0	0	1936
I(sp)		0.82	0.93	0.94	0.87	0.91		0.87	0.87	0.90			0.89
Potential experimental days	0	14	11	11.5	15	14	1	1	17	17.5	0	0	102.0
Real experimental days	0	9	8	11.5	14	13	0	1	15	17.5	0	0	89.0
I(ed)		0.64	0.73	1.00	0.93	0.93		1.00	0.88	1.00			0.87
Experimental minutes	0	2683	3631	4787	6075	4875	0	192	6355	8286	0	0	36884
Delay minutes	0	2455	1418	2378	2787	2979	0	207	2764	2618	0	0	17606
I(et)		0.52	0.72	0.67	0.69	0.62		0.48	0.70	0.76			0.68
A(sp/d)		16.78	25.63	21.48	22.29	21.69		13.00	21.67	22.21			21.75
A(p/d)		20.44	27.50	22.78	25.57	23.85		15.00	25.00	24.62			24.40

Delay per system (minutes)

	Jan.	Feb.	March	April	May	June	July	Aug.	Sept.	Oct.	Nov.	Dec.	Total	%
Machine	0	393	48	95	423	161	0	0	217	91	0	0	1428	8.1
Power supplies	0	552	205	289	477	665	0	0	410	386	0	0	2984	16.9
Radiofrequency	0	13	217	474	220	634	0	0	143	310	0	0	2011	11.4
Control system	0	260	256	206	320	261	0	35	310	208	0	0	1856	10.5
DAS	0	204	5	183	55	23	0	24	237	182	0	0	913	5.2
Feedback	0	41	65	6	98	188	0	0	0	0	0	0	398	2.3
Network	0	0	0	0	0	92	0	0	401	0	0	0	493	2.8
Diagnostic system	0	498	176	283	185	189	0	54	157	276	0	0	1818	10.3
Analysis	0	247	441	623	2001	633	0	0	717	995	0	0	4657	26.5
Others	0	247	5	219	8	133	0	94	172	170	0	10	1048	6.0
TOTAL		2455	1418	2378	2787	2979	0	207	2764	2618	0	0	17606	100

Summary of machine maintenance. Maintenance of the FTU systems was carried out according to schedule. At the end of June/October, the vacuum chamber was visually inspected. Only three old-type tiles were found broken inside the chamber, so the new solution adopted for installing the tiles in the support proved successful. Some problems with thyristors at the beginning of the year were solved, and more than 1000 shots were performed without any ruptures occurring.

New installations and changes. During the shutdown in the first part of the year, the new CO_2 interferometer system for electron density measurements was installed and successfully tested. Compared to the previous system, the new diagnostic enables measurements at higher density as well as a better reconstruction of the density radial profile, with good space and time resolution. A new fast valve was assembled on the lower hybrid antenna for coupling studies.

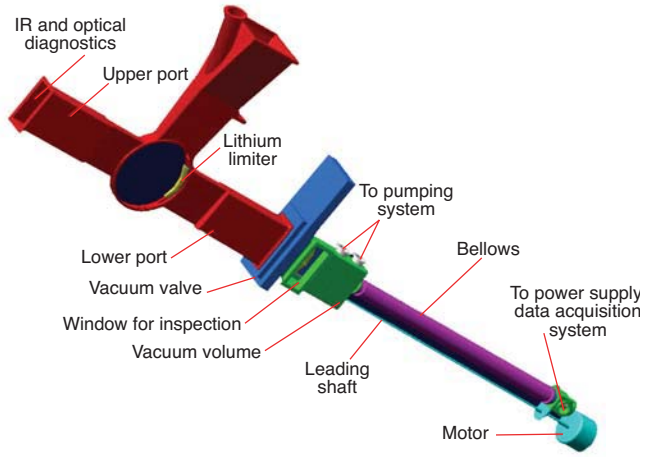

Fig. 1.3 - Schematic of the FTU sector, showing the three units composing the lithium limiter

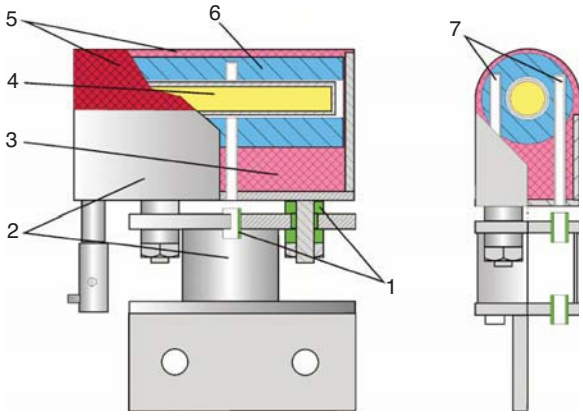

Fig. 1.4 - Main elements of the CPS structure: 1) ceramic break for insulating the unit from the support panel; 2) case with cylindrical support; 3) lithium-filled capillary structure; 4) heater; 5) lithium evaporating surface; 6) Mo heat accumulator; 7) seats for two thermocouples

Future activities. *Experiments on FTU with a liquid lithium limiter in a capillary pore system configuration.* An innovative solution proposed by Russian researchers at the Institute for Innovation and Fusion Research, Troitsk, Moscow [1.1] will be employed to investigate the use of liquid lithium as a plasma-facing component for the divertor target plates. The technique is based on the fact that the surface tension forces in capillary channels can compensate the jxB forces induced in lithium. This type of structure should have high stability and resistance, along with the intrinsic property of the plasma-facing surface to regenerate. The capillary pore system (CPS) limiter is a matt of stainless steel 304 wire mesh with pore radius 15 mm and wire diameter 30 mm. The liquid lithium flows inside these capillaries from one side of the system, which is in contact with a liquid lithium reservoir, to the other side facing the plasma. The high plasma densities (up to 3.2×10^{20} m^{-3}), high currents (up to 1.6 MA) and high magnetic fields (up to 8 T) attainable on FTU make it an ideal machine for carrying out the first tests on the CPS configuration in an ITER-relevant experiment. The liquid lithium limiter will evaporate during a plasma discharge from a thin-film wall coating by controlled displacement of the last closed magnetic surface. It will be possible to study important physical and technological issues, such as the wall conditioning efficiency of the lithium film in reducing plasma contamination and recycling, lithium accumulation and distribution inside the plasma, stability and resistance of the CPS in stationary regimes and during plasma disruptions, liquid lithium erosion in high-magnetic-field tokamak conditions and the reduction in the thermal load on the limiter because of the high latent heat of lithium vaporisation.

To optimise the system configuration and verify its feasibility on FTU, exhaustive calculations, developed by ENEA in collaboration with L.T. Calcoli, were carried out and then implemented by the Troitsk Institute together with the State Enterprise “Red Star” of Moscow in the framework of a contract to supply two lithium limiters for FTU. Thermal stress analyses in stationary and transient conditions showed that the ITER structural-criteria limits for all the materials are satisfied. Electromagnetic (em) calculations showed that lithium is well confined in the CPS structure, also in the presence of hard disruptions (I_p=1.6 MA, B_T=8 T), and that the contribution of em forces to the total stresses is within the structural-criteria limits [1.2]. Following these positive results, a prototype of the lithium limiter was developed and successfully tested in the laboratory, and the manufacture of two lithium limiter sets was started (figs. 1.3, 1.4). Installation and first experimental tests on FTU are planned for the second half of 2005.

1.2.2 Diagnostics

New scanning CO_2 interferometer for density measurements [1.3]. This diagnostic was developed by the Reversed Field Experiment (RFX) Consortium, assembled and tested under a collaboration between FTU and RFX, and installed in FTU at the end of 2003. This is the first scanning interferometer ever used in a tokamak system.

A resonant tilting mirror placed at the focus of a fixed parabolic mirror is used to scan the laser beams within the vertical port (fig 1.5). A CO_2 laser (10 W, λ=10.6 μm) is the main radiation source, while a CO laser (1 W, λ=5.4 μm) serves to compensate for mechanical vibrations. These wavelengths were chosen because of the very high densities (of the order of 10^{21} m^{-3}) reached with multiple pellet injection. The CO_2 and CO beams are modulated by two Bragg cells at 40 and 30 MHz, respectively, so that only one photoconductive detector, instead of two, is needed to detect their interferometric signals [1.4]. The two colour signals are separated electronically. A full profile is scanned in 42 μs.

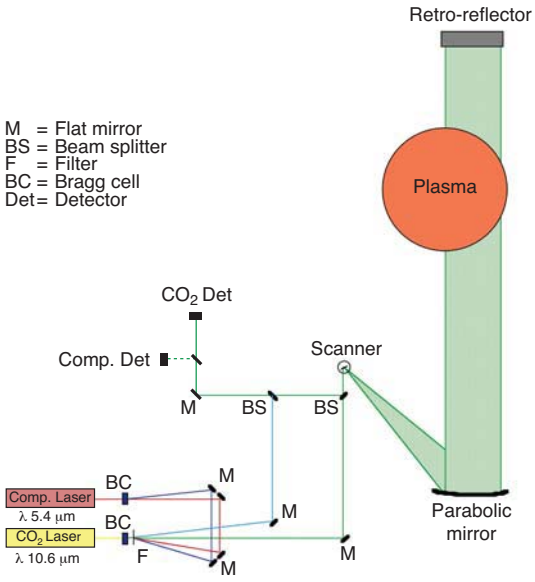

Fig. 1.5 - Sketch (not to scale) of the FTU scanning interferometer

Two independent scanning beams, at a scanning frequency of 12 kHz, were initially used to cover the full width of the FTU vertical port, providing 28-34 independent chords with a spatial resolution of about 1 cm. Due to an obstruction in the vertical port, one beam had to be excluded because it was difficult to reconstruct the correct phase crossing the obstruction. Three fixed chords are included in the apparatus. One of the chords passes through the centre of the chamber and is used for plasma density feedback control.

The scanning chord is shown schematically in figure 1.5. The CO and CO_2 beams are split in two by the Bragg cells and superimposed on an optical filter. Two visible laser beams are also superimposed on the infrared beams for alignment purposes.

One of the beams is deflected by the scanner and sent to the plasma by a parabolic mirror so that the beam translates vertically in the plasma. The beams are reflected back to the scanner by a “roof-top” retro-reflector made up of two rectangular flat mirrors forming a right angle. The deflection is cancelled with a second reflection on the tilting mirror. The scanning mirror has to be positioned with particular care at the geometrical focus of the parabolic mirror to ensure minimum variation in the optical path and complete cancellation of the deflection. Perfect alignment is obviously impossible and also the tilting movement of the “roof-top” mirror anchored directly to the tokamak flanges introduces a limit on alignment quality. The beam is then recombined with the reference beam by a beam splitter, and their interference is detected by a photoconductive detector.

Data acquisition is based on a compact peripheral component interconnect (PCI) crate controlled by a PC. Seven analog-digital converter (ADC) cards (INCAA CP-TR32-5026), with four channels at 3 MHz and 256 Mb memory on board, are

References

[1.1] V.A. Evtikhin et al., Plasma Phys. Control. Fusion **44**, 955 (2002)

[1.2] M.L. Apicella et al., *Proposal of experiment on FTU with a liquid lithium limiter in CPS (capillary pore system) configuration*, presented at the 23rd Symp. on Fusion Technology – SOFT (Venice 2004) Poster P4CF274

[1.3] O. Tudisco et al., Fusion Sci. Technol. **45**, 3, 402 (2004)

[1.4] A. Canton et al., Rev. Sci. Instrum. **72**, 1, 1085 (2001)

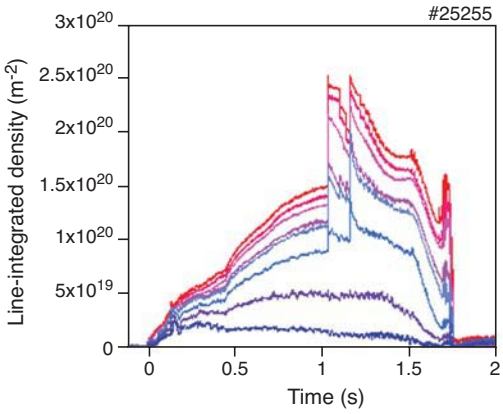

Fig. 1.6 - Line-integrated density at selected chords

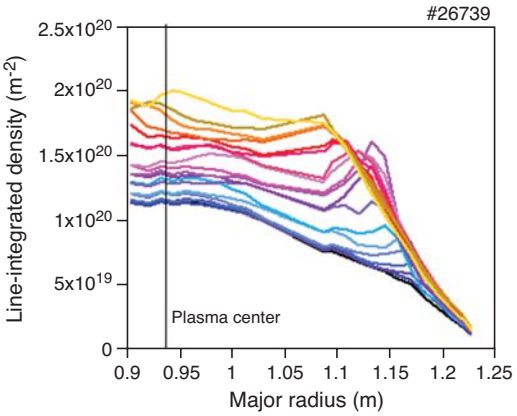

Fig. 1.7 - Line-integrated profiles during the penetration of a slow pellet

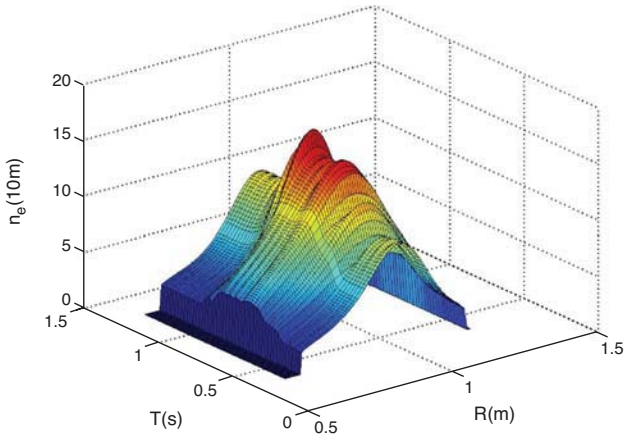

Fig. 1.8 - Time evolution of inverted density profiles in a 3D graph. The fast increase in density is due to pellet injection

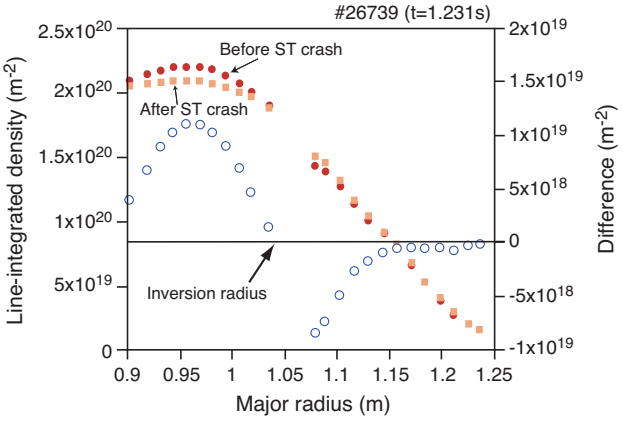

Fig. 1.9 - Effect of a sawtooth crash on the line-integrated profile and the difference in the two profiles. The inversion radius is clearly visible

used for acquisition. The fixed chords have an acquisition rate of 200 kHz, the scanning chords, 1.5 MHz, so 73 Mb are stored for each tokamak pulse.

At present only remote monitoring of the interferometer is possible, but remote control of the complete interferometer is being installed. The control system will be able to read and set the laser power, check the signal levels and optimise pre-amplifier gains, and diagnose the status of components (temperature, water cooling flux, etc.). It will also be possible to remotely perform fine alignment of the beams. The superimposition of the two colours can be controlled by means of a set of purposely installed detectors and mirrors.

The scanning-chord data can be processed either as a single chord up to the density calculation and then separated into independent fixed chords, or separating the raw data into low-frequency sampled signals (the scanning frequency) to be processed as fixed chords. Both methods have to be used to get a good reconstruction of the density in all the discharges.

During the two experimental campaigns of 2004, data were routinely produced in different FTU scenarios. Plasmas with internal transport barriers, obtained with lower hybrid current drive (LHCD) and electron cyclotron resonant heating (ECRH), and pellet enhanced performance (PEP) regimes sustained by multiple pellet injection were diagnosed.

A potential disadvantage is the non-simultaneity of the measurements because of the finite time scan. If the plasma is steady state within the scan time, the problem can be neglected and an inversion of the line integrated profile can be performed, assuming the density as a function of magnetic flux (Ψ), with the Cormack technique [1.5]. Figure 1.6 shows the density evolution at selected chords.

Particular attention has been paid to analysing pellet fuelled discharges [1.6], in which very peaked profiles are obtained. During the penetration of relatively slow pellets injected from the high-field side, the evolution of the profiles can be followed (fig. 1.7) and, as the penetration time is slower than the scan time, profile inversion can be carried out. Figure 1.8 reports the 3D evolution of inverted density profiles during pellet injection; figure 1.9 shows the effect of a sawtooth crash on the line-integrated profile after a pellet.

Neutron diagnostics update. The IDL programme for analysing FTU neutron data was completely rewritten in order to obtain Abel inversion of neutron brightness data from the FTU neutron camera by using flux coordinates. The programme now determines the ion temperature profiles derived from inverted density and inverted neutron emission profiles. Analysis of neutron camera data for a set of selected discharges showed agreement within about 15% between the total neutron yield measured by the neutron camera and that measured by the neutron yield monitors (BF_3 and fission chambers).

1.2.3 Additional heating systems

ECRH system. The ECRH system (140 GHz, 1.6 MW for 0.5 s) was used at 75% of its maximum power level for the entire 2004 campaign. Following the previous technical failures, three gyrotrons, with an improved version of the collector and cathode design, were tested and installed to complete the system. With the four gyrotrons in operation it was possible to achieve full power up to a record level of 1.5 MW coupled to the plasma (fig. 1.10), but a fault in a filament heater caused the available power to drop to 1.2 MW for the rest of the campaign. A new passive adaptation network inserted at the end of a high-voltage cable increased the stability of operations, while a new remote control procedure to allow tube conditioning on the loads in between plasma pulses improved system reliability.

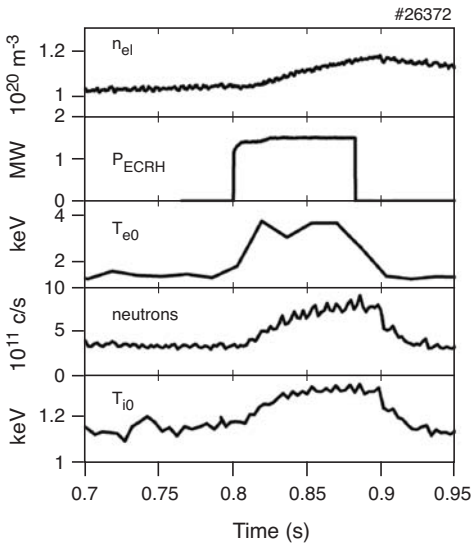

Fig. 1.10 - Time traces of the main signals of shot #26372 (B_t=5.3T, I_p=0.5MA). With 1.5 MW of ECRH power at $n_{e0}=1.6 10^{20} m^{-3}$, T_e increases from 1.8 to 4 keV and the neutron rate is multiplied by ~3, corresponding to $\Delta T_i/T_i$=25%

1.3.1 Progress in high-density internal transport barriers in FTU

In 2004 the programme on internal transport barriers (ITBs) was focussed on the formation and characteristics of steady ITBs at high plasma density (n_e). Unlike most tokamaks, FTU simultaneously meets the essential ITER requirements of high n_e, dominant electron heating and negligible momentum injection. Steady barriers up to central values $n_{e0}>1.4\times10^{20}$ m^{-3} are produced through LHCD and electron cyclotron heating (ECH) only. The crucial questions examined are whether the collisional electron-ion (e^--i^+) coupling, which is of utmost importance in ITER, degrades the ITB quality by

References

[1.5] A.M. Cormack, J. Appl. Phys. **34**, 2722 (1963) and J. Appl. Phys. **35**, 2908 (1964)

[1.6] D. Frigione et al., *Pellet injection from the high field side on FTU*, presented at the 31st Eur. Physical Society Conf. on Plasma Physics (London 2004)

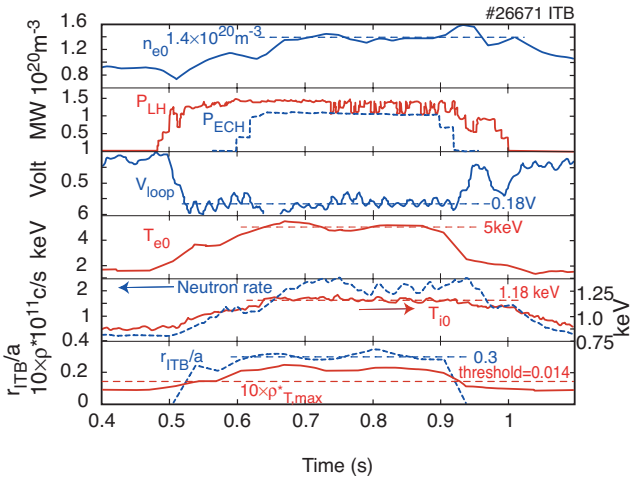

Fig. 1.11 - Time evolution of the most significant macroscopic plasma parameters for discharge #26671 (the steady ITB at the highest density)

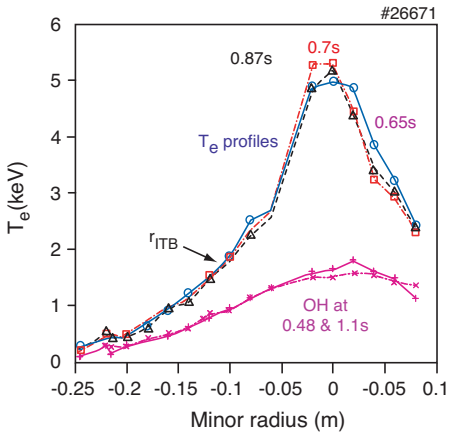

Fig. 1.12 - Electron temperature profiles in Ohmic and ITB phases for discharge #26671

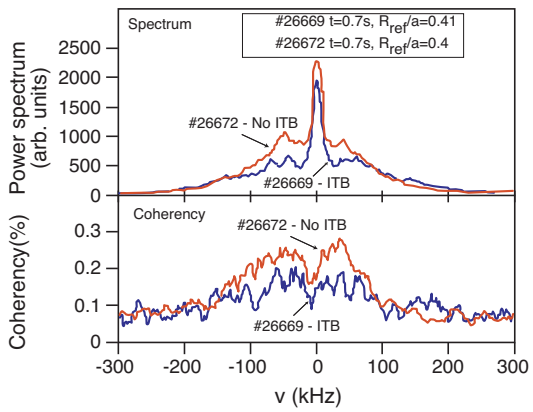

Fig. 1.13 - Fluctuation power spectra (above) and coherence spectra (below) for two discharges with ITB (#26669) and without (#26672); $n_e \approx 0.9\times10^{20}$ m^{-3} for both

affecting the turbulence stabilisation mechanisms producing electron ITBs (e-ITBs) and whether a barrier on ion transport can even be built by electron heating methods. The latter issue is very relevant for ITER because so far ion transport has been depressed only when the plasma rotates.

Internal transport barriers are formed in FTU in a large range of plasma parameters, namely, line-averaged density $0.3\leq n_e\leq1.1\times10^{20}$ m^{-3}, plasma current $0.35\leq I_p\leq0.7$ MA and toroidal magnetic field $5.2\leq B_T\leq7.2$ T [1.7]. The only requirement to be satisfied is to drive enough current off-axis to create a safety factor radial profile q(r) with a central value $1<q_0<2$, followed by a shearless or inverted shear region with $q_{min}\approx1.2$-1.3. This avoids harmful magnetohydrodynamic (MHD) activity, such as double tearing modes at the q=2 surfaces or sawteeth. Mild m=1 activity is, instead, often present in ITBs, with possible beneficial effects against impurity accumulation. These q profiles are quite similar to those typical of hybrid regimes [1.8] and are even steadier, essentially because they do not need any mechanisms to prevent diffusion of the current, which is mostly fixed by an external drive. Duration longer than $35\tau_E$ (with τ_E the global energy confinement time) and about $1.5\tau_{R/L}$ (with $\tau_{R/L}$ the Ohmic current relaxation time) has been achieved [1.9]. No significant difference is observed in the construction of such steady q profiles, whether LHCD is applied during either the I_p plateau or the ramp-up phase, mainly because various constraints do not allow LH power to be injected at the very beginning of the discharge, when the actual q profile is very far from relaxed [1.9]. Both LHCD and ECH are also the heating sources for the bulk plasma.

As density increases, ECH offers valuable twofold assistance to LHCD in sustaining proper q profiles. Regardless of the toroidal injection angle, it enhances the LHCD efficiency by increasing the plasma temperature, whereas in the counter electron cyclotron current drive (ECCD) configuration it can provide a small but centrally well localised counter current drive, leading to a slightly reversed q profile suitable for an ITB. The use of central ctrECCD was essential to build a steady ITB at the highest density obtained so far in FTU (fig. 1.11). Otherwise, a marginal ITB is obtained if ECH is launched perpendicularly to B_T, or sawteeth reappear and an ITB is not built at all

in a coECCD configuration. Figure 1.11 shows that an almost full current drive (V_{loop}<0.2 V, Ohmic current <20%, duration ≈15τ_E or ≈1$\tau_{R/L}$) is sustained for the whole duration of the ECH pulse at n_{e0} and T_{e0} exceeding 1.4×10^{20} m^{-3} and 5 keV, respectively. The fusion neutron rate is ten times higher than it is in the Ohmic phase for a central ion temperature increment of more than 35%. However, the still long thermal e^-–i^+ equipartition time τ_{ei}≈180 ms, with τ_E≈22 ms, does not allow T_i to approach T_e. The strength of the barrier given by $\rho_T^*=\rho_{L,s}/L_T$, where $\rho_{L,s}$ is the Larmor radius of the ions moving at sound velocity and $L_T=T_e/(dT_e/dr)$, is > 0.02, well above the threshold value of 0.014, and it remains constant, as do all the other ITB relevant features. According to the hard x rays perpendicularly emitted via Bremsstrahlung by the LH-generated fast electrons, the q profile always maintains a mildly reversed shape in the centre, with q_0>1.5 and q_{min}≈1.2. As shown in figure 1.12, no variation in the T_e profile, and hence in ρ_T^*, is observed. Consequently, the ITB radius, i.e., where ρ_T^*=0.014, remains fixed at r_{ITB}/a≈0.35 (a=plasma minor radius), where q_{min}≈1.5 and the shear is quite small. Weak MHD activity, m=3 n=2, is observed, which is consistent with a double tearing mode developing at the two radii where q(r) crosses the value of 1.5. The ITB foot is very often located close to where q has a simple rational value and the magnetic shear is quite low. This latter feature facilitates good alignment of the bootstrap and driven currents in LH-generated ITBs. Indeed, the largest modification of the shear occurs close to the radial LH deposition peak, and it is right there that the steep pressure gradient originating the bootstrap current starts. I_{bs}/I_p>30% has been achieved in FTU, against the target of 50% required for ITER (I_{bs}/I_p ≥20% for the case of figure 1.11).

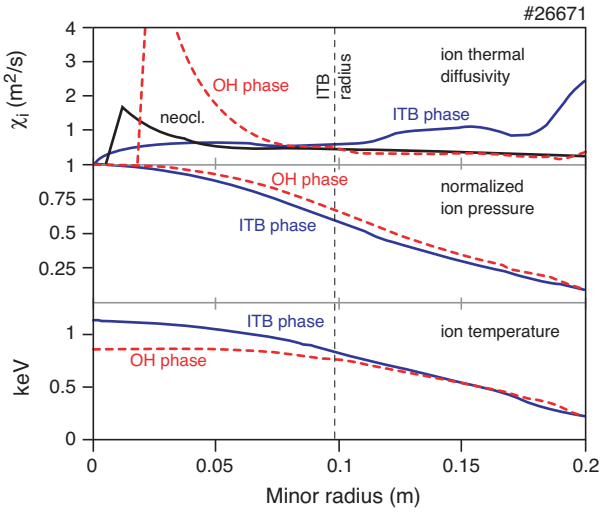

Fig. 1.14 - Comparison of ion behaviour in Ohmic and ITB phases for discharge #26671. Top frame: ion thermal diffusivity radial profile χ_i(r): the neoclassical level is attained during the ITB. Middle and bottom frames: normalised ion pressure and ion temperature profiles, respectively

The first direct evidence of a change in the nature of the turbulence when an ITB is built was recently obtained just in a high density case. Measurements with a two-channel fixed-frequency reflectometer show a remarkable reduction both in the fluctuation and in the coherence power spectra when an ITB is built, as pointed out by comparison with a non-ITB discharge (fig. 1.13). The two discharges are identical except for the fact that the non-ITB discharge lacks ECH power. Since the reflection radius is located just at the ITB foot, phenomena linked to reduced transport are observable in FTU even outside the ITB zone, in disagreement with the DIII-D claims that turbulence is stabilised only inside the ITB [1.10]. The reasons for such observations are being examined. The 5° poloidal separation between the two viewing chords corresponds to $k_\theta\rho_i$ in the range ≈0.2-0.3 (ρ_i=ion Larmor radius, k_θ=poloidal wave vector), which is a scale length at the boundary between the ion temperature gradient and trapped electron modes.

While the drop in electron heat conductivity in electron ITBs has been well assessed [1.7], the drop in ion thermal diffusivity to an almost neoclassical level (fig. 1.14) has only recently been identified after obtaining reliable T_i profiles from the neutron multicollimator, which have also been validated by x–ray curved-crystal data. This confirms the early assumptions about lower density and power [1.11] and accounts for the global ion behaviour inside the ITB, i.e., the tenfold neutron

References

[1.7] E. Barbato et al., Fusion Sci. Technol. **45**, 3, 323 (2004)

[1.8] C. Gormezano et al., Plasma Phys. Control. Fusion **46**, B435 (2004)

[1.9] V. Pericoli Ridolfini et al., Nucl. Fusion **43**, 469 (2003)

[1.10] E.E. Doyle et al., Nucl. Fusion **42**, 333 (2002)

[1.11] C. Castaldo et al., Proc. 29th EPS Conf. on Plasma Phys. and Contr. Fusion (Montreux 2002), ECA V. 26B, O-1.04 (2002)

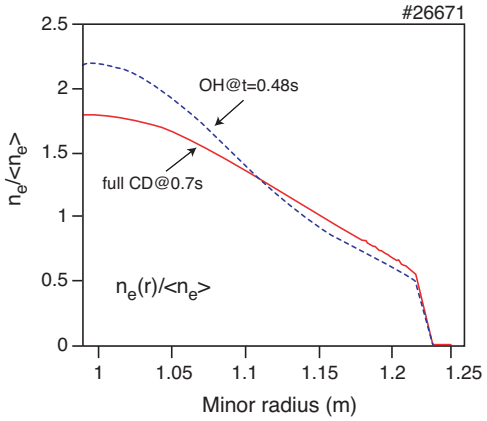

Fig. 1.15 - Normalised density profiles in Ohmic and almost full current drive phase for discharge #26671, showing that the profile remains quite peaked even without the particle Ware pinch

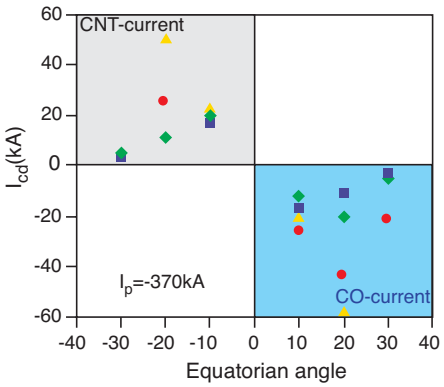

Fig.1.16 - ECCD vs. injection angle in FTU. Comparison of different measuring techniques: (blue) the result of the EGBW code; (red) I_{ECCD} from volume-integrated formula; (green) from comparison of similar co-counter shots ; (yellow) from neoclassical resistivity calculated from n_e, T_e profile. B_T is arranged for central deposition (from 4.8 to 5.2T), I_p=350 KA and line-averaged electron density is 0.7×10^{20} m^{-3}

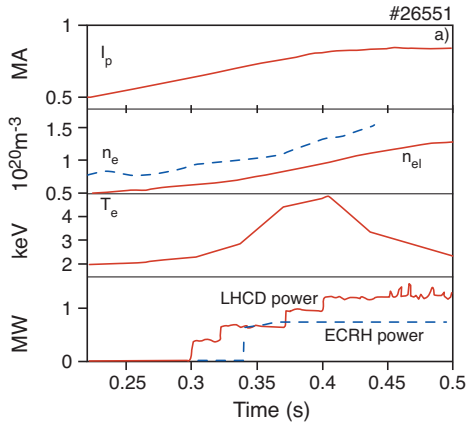

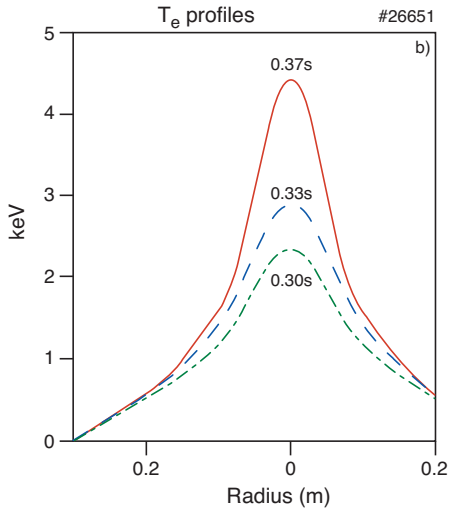

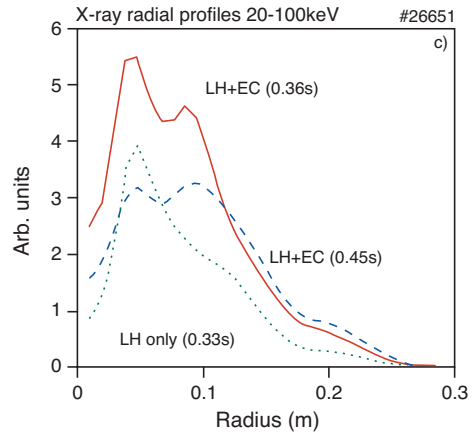

Fig. 1.17 - a) Main signals of shot #26551. LHCD and ECRF are applied during the ramp-up phase of a 0.8-MA, 7.2-T pulse. An ITB is not maintained when the density is too high. Plotted are the line-averaged density (n_{el}) and the central density (n_{e0}). b) Electron temperature profiles (from Thomson scattering) in shot #26651 during the pre-heat phase (t=0.30 s, dash-dot line), the start of EC+LHCD phase (t=0.33 s, dashed line) and at t=0.37 s (solid line) when the ITBs start to collapse when the density is too high. c) Radial inverted HXR signals from the FEB camera for shot #26651 during the LHCD-only phase (t=0.33 s, dotted line), the start of EC+LHCD phase (t=0.36 s, solid line) and at t=0.40 s (dashed line) when the ITBs start to collapse when the density is too high. The integration time is about 20 ms

rate increase and the stronger ion heating with respect to an Ohmic case with very similar density and e^-–i^+ collisional coupling [1.9]. Particle transport in almost full current drive conditions [1.12] gives in turn good expectations for peaked density profiles in ITER ITBs, where central particle fuelling is very problematic and the Ware pinch mechanism will be very weak due to the low (or null) toroidal electric field. Indeed, in very similar conditions the density profile in FTU maintains quite a high peaking factor. As shown in figure 1.15 (same discharge as in fig. 1.11), $n_{e0}/\langle n_e \rangle$ remains above 1.7, larger than the figure quoted (≈1.3) for other devices, such as JET [1.13] or ASDEX Upgrade [1.14], for similar values of the adimensional collisionality ($\nu_e^* \approx 0.2$ at r_{ITB}).

The FTU results then indicate that operations close to n_e and B_T of ITER and electron-ion collisions do not prevent ITBs from being achieved. The collisional heating of ions produces $\Delta T_{i0}/T_{i0}>35\%$ and a tenfold increase in the fusion neutron yield, with a drop in heat diffusivity to the neoclassical level and below the Ohmic phase. A reduction in the fluctuation amplitude at the barrier radius is observed to be closely correlated with the onset of the ITB, together with a decrease in coherence between two regions 5° poloidally apart, which is consistent with a reduction in the turbulent spectrum in the medium-low k_θ range.

1.3.2 ECRH experiments

Electron cyclotron current drive results. Preliminary ECCD experiments have been performed at P_{EC}=1.2 MW to establish the related database on FTU. For a complete first-pass absorption, the plasma parameters were $0.5<\bar{n}_e<0.6\times10^{20}m^{-3}$ and $3<T_e<5$ keV. A series of experiments with the toroidal injection angle set at ±10°, ±20°, ±30° (off the radial direction) allowed a first assessment of the driven current in discharges with I_p up to 400 kA and $2.5<Z_{eff}<3$.

The electron cyclotron driven current was calculated both through the plasma resistance (using neo-classical resistivity) and from comparison of co- and counter-experiments, considering the difference in ΔV_{loop}. The resulting I_{ECCD} is given in figure 1.16, where results of the different techniques are compared with theoretical calculations. The values of up to 15-20 kA (at the best angle of ±20°) obtained are in agreement within ±10% with linear theory calculations performed with the electron cyclotron wave Gaussian beam (ECWGB) code, which is a satisfactory output for these very first experiments at FTU [1.15].

Synergy experiments. Electron ITBs at high densities and high magnetic field (B_t=7.2 T) have been produced using synergy between electron cyclotron resonance frequency (ECRF) and LHCD in the down-shifted resonance absorption scheme. In these experiments the electron cyclotron wave can be absorbed by the fast electron tail generated by LHCD through the Doppler shift [1.16], even if the cold resonance (B_0=5 T) is outside the vacuum chamber. This effect has already been documented for FTU [1.17]. In 2004 experiments with ECRH were used to enhance the current drive generated by lower hybrid waves. Almost full current drive was achieved at B_t=7.2 T, I_p=0.5 MA and $n_{e0}=0.9\times10^{20}$ m^{-3} with 1 MW of LHCD and 1.1 MW of ECRF power, while the hard-x-ray (HXR) signal from the fast electron (50-200 keV) Bremsstrahlung (FEB) camera was doubled during ECRF application. As shown in figure 1.17a, an ITB was triggered by electron cyclotron suprathermal absorption during the ramp-up phase of a 7.2T/0.8 MA pulse at a central density in excess of $n_{e0}=1.0\times10^{20}m^{-3}$, as shown by the electron temperature

References

[1.12] M. Romanelli et al., *Studies of confinement and turbulence in FTU high field high density plasmas,* presented at the 20th Fusion Energy Conf. (Vilamoura 2004)

[1.13] H. Weisen et al., *Anomalous particle and impurity transport in JET*, presented at the 20th Fusion Energy Conf. (Vilamoura 2004) IAEA-EXP/6-31

[1.14] S. Gunther et al., *Overview of ASDEX Upgrade results*, presented at the 20th Fusion Energy Conf., (Vilamoura 2004)

[1.15] S. Nowak, E. Lazzaro and G. Ramponi, Phys. Plasmas **3**, 4140 (1996)

[1.16] G. Granucci et al., Fusion Sci. Technol. **45**, 387 (2004)

[1.17] B. Angelini et al., Nucl. Fusion **43**, 1632 (2003)

profiles (fig.1.17b). The radial inverted HXR signals from the FEB camera are shown in figure 1.17c. When ECRF is applied, spectra are substantially enhanced initially, but are subsequently reduced because of the increase in density during the current ramp-up phase, which leads to a reduction in energetic electron population. As a consequence, the less effective damping of the electron cyclotron waves reduces the amount of non-inductive current drive and, hence, the ITB is lost, at least at the available power level of these experiments. In effect, at t=0.36 s, the electron cyclotron power coupled to the fast electrons is estimated to be about 50%, while when the density increases the coupled electron cyclotron power decreases (by about 40%), the HXR spectrum is reduced and the ITB cannot be maintained. Higher power would be necessary to maintain e-ITBs in these high-density/high-current plasmas.

Collective Thomson scattering (CTS) experiments. In 2004 significant technical and methodological improvements were implemented on the 140-GHz CTS diagnostic experiment supporting the investigation of anomalous spectra systematically detected in previous campaigns. A movable probe carrying a linear array of sensors and purposely inserted in the plasma vessel allowed better control and good reproducibility of beam alignment (scattering volume). Optimised rejection of the stray radiation was achieved by the innovative procedure of finely matching the gyrotron frequency to the central frequency of the notch-filter. A number of operations, including frequency matching, measurement of the gyrotron noise spectrum, and accurate calibration of the 32-channel radiometer by ECE, were greatly facilitated by the implementation of a remotely controlled synthesizer and a new multi-purpose front-end.

Experiments with P_{rf}=300 kW for 200 ms were performed during the ramp-up phase of high-performance plasmas (B_0=7.2 T, I_p=1.1 MA). The anomalous spectra, observed also in these shots, were definitely ascribed to plasma-wave interaction.

Both a 1/f-like feature and a complex line structure can be distinguished in the observed spectra. Partially overlapping but sufficiently well-resolved harmonics of the central ion cyclotron frequency (nf_{ci0}) for a B_0=7.2 T deuterium plasma (f_{ci0}=56 MHz) were observed up to n=7 in the lower half ($50 \leq f \leq 500$ MHz) of the detection range where narrower channel widths allow higher resolution. For long enough interaction times, the ion cyclotron lines decay and the spectra reduce to the smooth 1/f-like feature. A sensible dependence on beam polarization was manifest in a reduced (±20°) polarization scan. While an exhaustive analysis of these data will require time and effort, an attempt to define the underlying scenario is under way to provide guidelines for the ongoing work.

1.3.3 Lower hybrid reflection coefficient control system

It is well known that the coupling conditions between a grill and a plasma depend mainly on the electronic density and its decay length in the scrape-off layer (SOL). These quantities are complex functions of several plasma and first-wall parameters. It can be shown by a simplified model of the plasma-SOL-antenna system that, for any given density gradient in the SOL and launched spectrum, the reflection coefficient is a convex function of the density in front of the antenna and then of its position inside the SOL.

Within this frame it is possible to envisage a control scheme based on real-time control of the position of the last closed surface (LCS) in order to minimise the reflection coefficient.

The problem of “search for a minimum” has been widely analysed, taking into account the theoretical and numerical approach of the properly called extremum seeking method. By exploiting the convex shape of the “transfer function”, the input (the LCS position in the present case) of the system can be perturbed by a “sinusoidal” signal. On the negative slope branch of the function, the output signal (the reflection coefficient in this case) will be a sinusoid with opposite phase. On the other branch the sinusoid will be in phase. The input and output signals are processed by a bandpass filter to enhance the driving frequency and multiplied and processed by an integrator with saturation and gain control. The output will be the correction signal to the reference (the reference of the LCS position). The scheme is summarised in figure 1.18.

In the second half of 2004 a preliminary control system based on Versa Module Eurocard (VME) hardware architectures was realised. A 16-channel analogue-digital converter acquires the direct and reflected lower hybrid power measured by a subset of eight waveguides of the entire grill (48 waveguides, see fig. 1.19). A central processing unit (CPU) deals with data acquisition and the computation of the reflection coefficient. The datum is transferred to the main control system of the FTU experiments, which generates the reference waveform that drives the different coils and controls, in particular, the external radius of the LCS.

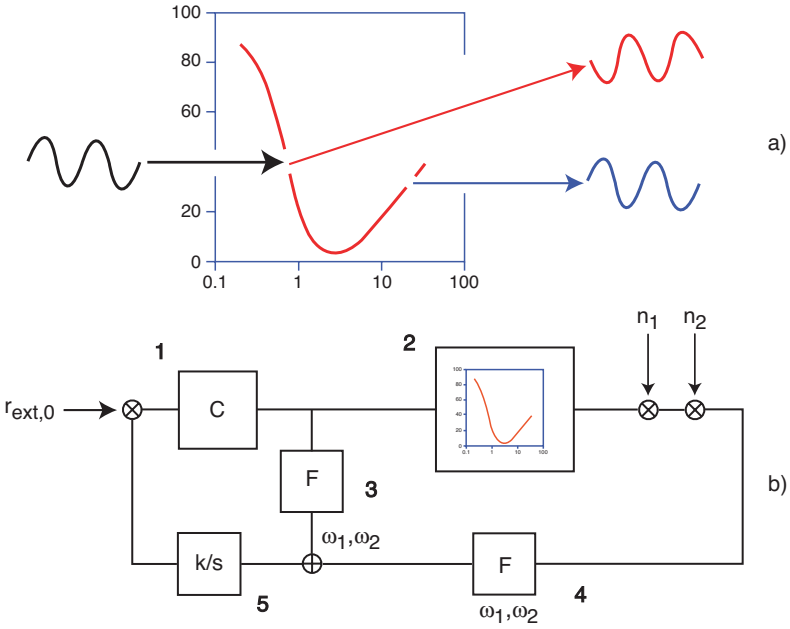

Fig. 1.18 - a) Convex property of the transfer function induces different phasing on the reflection coefficient after a "sinusoidal" perturbation on the LCS position. b) Control scheme: r_{ext} external radius of LCS reference signal; 1 - control coils of the external radius; 2 - convex transfer function, n_1, n_2 noise sources; 3 and 4 - bandpass filter; 5 - integrator with saturation and variable gain

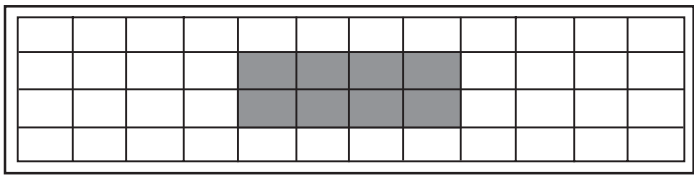

Fig. 1.19 - Schematic of the LH launching grill of FTU: shadowed portion shows where the direct and reflected power is measured

At this very early stage external perturbative methods are not used. A preliminary study on the quality of the signals involved in the control loop demonstrated that the current of the relevant coil shows a set of harmonics, the strongest being about 50 to 60 Hz (a residual of rectifier circuits). This "natural" oscillation induces a sensible oscillation of the external radius, which can be used in the control scheme. Figure 1.20 summarises the results of a series of experiments aimed at precise tuning of the different feedback parameters (bandpass frequency 20-100 Hz, gain and saturation of the integrator). In the figure the external radius of the LCS actually obtained is the violet waveform. The correction saturates due to safety limits imposed on the values required from the control system. Reference is made to shot #26725 because this was the first time a complete evolution in the control of the external radius was recorded, that is, the control system reaches and exceeds the minimum of the convex function, then correctly drives the inversion of the displacement.

The system is now applied to one of the six lower hybrid launchers of FTU. The launchers are divided in two groups, placed at different toroidal positions. In each group the three launchers are poloidally distributed and rigidly connected. In future experiments it is hoped to establish what effect the poloidal anisotropy of the coupling has on the remaining two grills by maintaining control on only one of the grills. The second obvious step is to extend the control to the remaining systems and, in the case of incorrigible poloidal anisotropy, to try and include in the control scheme the coil which is related to the vertical position of the LCS.

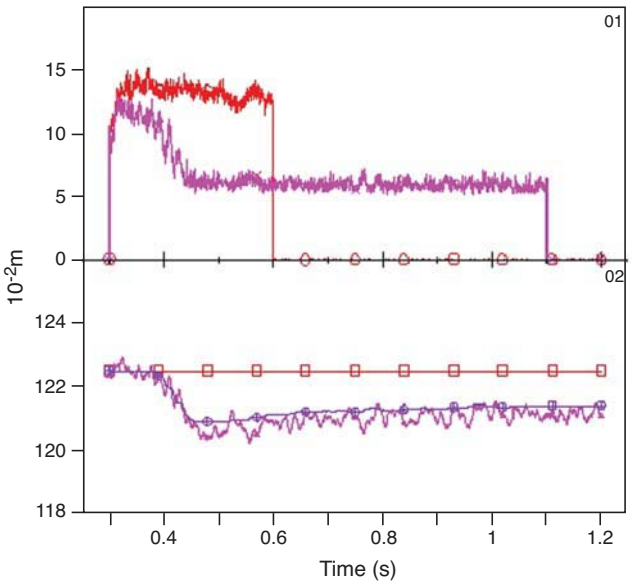

Fig. 1.20 - Preliminary results of LH reflection control: a) Comparison between reflection coefficient without control loop (red) and with control loop (violet), with control starting 30 ms after LH switch-on; b) pre-programmed external radius of LCS (red, squares) and superimposed correction of control system (blue line, circles and crosses)

1.3.4 MHD studies

Slow sawtooth reconnection in the hybrid advanced mode of operation. Fast magnetic reconnection is commonly observed during sawtooth collapses in tokamaks. The reconnection time scale is orders of magnitude faster than the resistive time scale proposed by Kadomtsev, and numerous theoretical studies have been devoted to reconciling this discrepancy by including electron inertia and compressibility effects.

On the other hand, very slow sawtooth reconnection has been observed in recent experiments on the hybrid regime at JET [1.18]. The magnetic island formed by reconnection grows exponentially with an e-folding time of 90 ms (fig. 1.21), which is longer than the Kadomtsev time (about 30 ms). The distinctive feature of these experiments was the presence of a wide central region with low magnetic shear and $q_{min} \approx 1$. The q profile was tailored by adjusting LHCD power and by properly timing the onset of the main heating (neutral beam injection plus ion cyclotron resonance heating). Slow pulsations of magnetic activity with n=1 toroidal mode were observed during the main heating. Soft-x-ray and ECE analysis demonstrated that this activity is due to the formation of a magnetic island at the q=1 radius. Central temperature slightly decreased during each pulsation, but no fast crash was observed. The observation of slow reconnection in plasmas with low magnetic shear, in contrast to fast reconnection in plasmas with higher shear in the plasma core, indicates that a threshold in magnetic shear could be the critical element for the onset of fast magnetic reconnection.

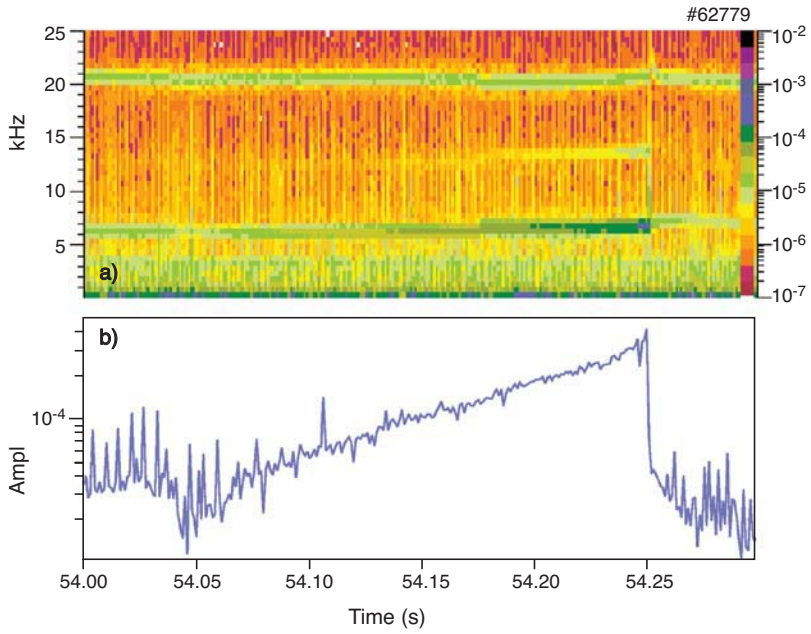

Fig. 1.21 - Evolution of magnetic oscillations during slow reconnection in JET pulse #62779. a) Spectrogram showing n=1 oscillations at 7 kHz, a weak n=2 second harmonic, and a persistent n=3 NTM at 21 kHz. b) Amplitude of the n=1 component in log scale; the constant slope between t=54.1 s and t=54.25 s corresponds to an e-folding time of 90 ms

Progress in the analysis of high-frequency modes in FTU. A new plasma phenomenon discovered on FTU is the generation of high-frequency (HF) oscillations by large magnetic islands [1.19,1.20] with (-2, -1) poloidal and toroidal mode numbers. The relevant experimental observations can be summarised as follows: 1) HF modes only appear when the magnetic island reaches a threshold amplitude. 2) HF mode frequencies range from 30 to 70 kHz. 3) HF modes form standing-wave structures in the island rest frame (fig. 1.22). 4) HF modes are observed in Ohmic plasmas in which fast ions are absent.

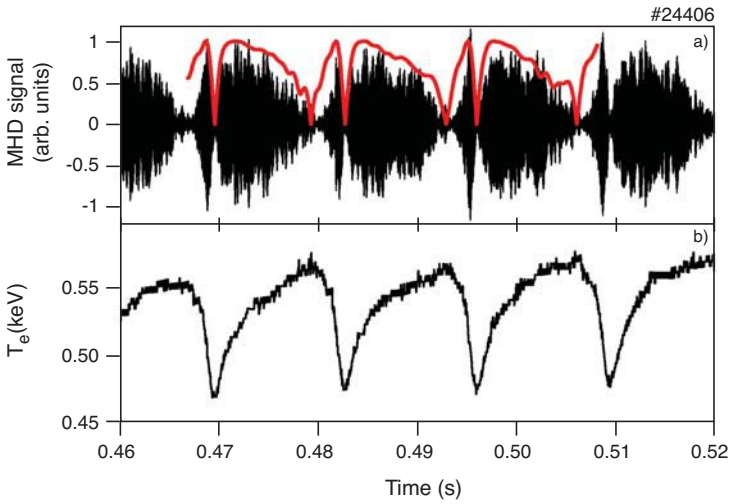

Fig. 1.22 - a) HF signals (42-53 kHz) from FTU magnetic coil #5 (16° above midplane) showing beating structure. b) Temperature oscillations at R=0.8 m from ECE, showing nonuniform island rotation. The red trace in a) shows the beat envelope as evaluated from the phase of signal b)

The frequency range of HF modes is inside the low-frequency gap introduced in the shear Alfvén continuous spectrum by finite beta effects, while the toroidicity-induced gap is one order of magnitude higher. Since in these Ohmic plasmas there are no fast ions that can excite Alfvén modes, the observed perturbations are likely to be due to the nonlinear excitation of shear-Alfvén waves by the magnetic island. More precisely, it is conjectured that modes of the beta-induced Alfvén eigenmode (BAE) branch are marginally stable in the case under investigation and can be nonlinearly excited in the presence of a sufficiently large magnetic island. The lowest order BAE angular frequency can be estimated by

$$\omega_{BAE} \cong \frac{1}{R_0}\sqrt{\frac{2T_i}{m_i}}\left(\frac{7}{4}+\frac{T_e}{T_i}\right)^{1/2}$$

i.e., by the accumulation point of the low-frequency gap introduced in the shear Alfvén continuous spectrum because of finite beta. This frequency is an upper bound for the expected mode frequencies, consistent with experimental observations; in fact, for deuterium ions with $T_i=T_e=0.5$ keV, one has $\omega_{BAE}/2\pi\cong 63$ kHz. Pairs of BAEs, with given helicity and localised near the q=2 surface, can interact with the (-2,-1) island via three-wave couplings and be nonlinearly excited provided that the energy transfer rate from the island to the BAEs be sufficient to overcome the linear mode damping, thereby setting a threshold condition for the island amplitude.

For each BAE propagating in the electron diamagnetic direction, the model predicts that there will be a twin BAE wave propagating in the ion diamagnetic direction. These twin waves will look like standing waves in the plasma rest frame, the phase coherence being set by the common nonlinear excitation mechanism, i.e., the (-2,-1) island. Detailed theoretical work is under way; for the moment, it can be stated that the present conjecture is in qualitative agreement with all the relevant observations.

Helical equilibria. Helical distortions of the axisymmetric

References

[1.18] P. Buratti et al., *Observation of slow sawtooth reconnection in JET low-shear discharges*, presented at the 31st EPS Conf. on Plasma Physics (London 2004)

[1.19] P. Buratti et al., Fusion Sci. Technol. **45**, 350 (2004)

[1.20] P. Buratti et al., *Observation of high-frequency secondary modes during strong tearing mode activity in FTU plasmas without fast ions*, presented at the 20th Fusion Energy Conf. (Villamoura 2004)

tokamak equilibrium have been systematically observed in FTU following injection of deuterium pellets [1.21,1.22]. Similar single-helicity states have been found in reversed field pinches, in conjunction with improved confinement. Since the observed distortions have large and steady amplitude, they have been studied as solutions of the nonlinear Grad-Shafranov equation in helical geometry [1.23]. Equilibria resulting from preliminary numerical calculations are in qualitative agreement with measured soft-x-ray maps.

MHD activity during high-power LHCD with ECCD. FTU discharges with high-power LHCD and counter ECCD show two central MHD modes oscillating at 15 and 10 kHz that are clearly observed on soft-x-ray signals and just visible on the Mirnov coils, and that have amplitudes $\delta B/B$ of 5×10^{-5} and 1.3×10^{-4}, respectively, relative to the poloidal field. The 15-kHz mode has two phase inversions on the soft x rays at r=2 cm and r=6 cm, indicating that two distinct islands rotating at a common frequency are present. Magnetic data give m=3 and n=1-2 for this mode. These results indicate that a pair of q=1.5 surfaces exist in the plasma.

1.4.1 Introduction

The first-principle-based theory of spontaneous excitation of zonal flows by ion temperature gradient (ITG) turbulence in non-uniform toroidal plasmas, developed in collaboration with the University of California at Irvine and the Princeton Plasma Physics Laboratory, has been applied to demonstrate that the ITG turbulence intensity level exhibits a transition from Bohm scaling at small system size to gyro-Bohm for large system size, and this transition is displayed by the fixed point solutions of the nonlinear ITG zonal flow system. Under the collaboration with the University of California at Irvine, a first-principle-based theory of nonlinear electron trapped gradient (ETG) dynamics was formulated as well, providing the basis for understanding and explaining recent results on ETG turbulent transport, suggesting that the electron heat conductivity is much smaller than the values of experimental relevance, at least for positive magnetic shear.

Existing numerical tools for rapid and reliable analyses of electrostatic drift wave microinstabilities have been upgraded to account for finite collisionality at high plasma density and have been extensively used for systematic transport studies in FTU as a complement of other routinely used transport codes, with particular emphasis on turbulent particle pinch.

Another theoretical activity closely connected with experimental campaigns both in FTU and in JET is modelling of lower hybrid wave (LHW) propagation in toroidal plasmas. Further developments of numerical investigation tools in this area are also discussed in the relative section. Ion cyclotron resonant heating scenarios in JET have been systematically investigated and the prerequisites for their analysis and development are discussed.

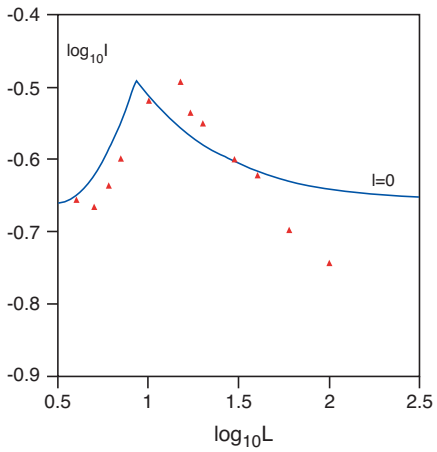

The theoretical analysis and reconstruction of the shape of an m=1 magnetic island, as observed in FTU, are also reported.

It has been demonstrated that fast ion transport in burning plasmas is characterised by a transition from weak (diffusive) to strong (ballistic) processes above a threshold in fast ion energy density that is close to the linear excitation threshold of energetic particle modes (EPMs). These findings

Fig 1.23 - Normalised ITG turbulence intensity I vs. the dimensionless length $L=|ndq/dr|\ (\gamma d/\omega)^{1/2}\ L_p$. Simulation results (red triangles) of numerical solutions of the ITG-ZF nonlinear equations derived in [1.30,1.31], compared with analytic predictions based on fixed-point solutions for the ground-state ITG radial envelope [1.36]

motivated studies on the alpha-particle behaviour in realistic ITER scenarios. The relative numerical investigations, done with the hybrid MHD gyrokinetic code (HMGC), demonstrated that strongly reversed plasma equilibria are unfavourable for the transport of energetic particles.

The final issue addressed here concerns distributing parallel computation in a grid environment, for the case of a particle-in-cell code (e.g., HMGC).

1.4.2 Zonal flow dynamics and anomalous transport

Anomalous transport in magnetically confined plasmas has been found to be significantly reduced by the existence of turbulence driven zonal flows (ZFs) consisting of narrow radial bands of poloidally rotating plasma, which reduce the radial coherence length of the fluctuations [1.24,1.25]. In 1998 Rosenbluth and Hinton [1.26] showed that linear collisionless processes do not damp poloidal flows driven by ITG turbulence. Shortly afterward these results were confirmed by large-scale numerical gyrokinetic calculations [1.27], which also showed that zonal flows could significantly reduce turbulence levels. To understand the interplay of zonal flow dynamics and turbulence levels, a local four-wave model was constructed by Chen, Lin and White [1.28]. This model, which can be extended from electrostatic fluctuations to electromagnetic [1.29], successfully captured the saturation of the turbulence, but being local could not predict the scaling of the saturation phenomenon with system size, (L_p/ρ_i), with L_p the equilibrium gradient scale length and ρ_i the ion Larmor radius. More recently, by assuming a hierarchy among nonlinear interactions, equations were derived [1.30,1.31] for the slow space-time evolution of the drift wave radial envelope and zonal flow structures, starting from the nonlinear gyrokinetic equation [1.32]. These equations incorporate the effects of equilibrium variations, i.e., turbulence spreading and size-dependence of the saturated wave intensities and transport coefficients [1.27,1.33-1.35], and they reduce to the local four-wave model in the limit of large system size. These equations are examined numerically and analytically. The nonlinear system converges to stable fixed points in the limit of weak drive both for small and for large system size. The turbulence intensity level exhibits a transition from Bohm scaling at small system size to gyro-Bohm for large system size, and this transition is displayed by the fixed-point solutions (fig. 1.23) [1.36]. For intermediate system size and for stronger drive, there is chaotic behaviour and intermittency [1.30]. However, in the chaotic domain, where the fixed points are unstable, the nonlinear behaviour is given by fluctuations about the fixed point, which therefore still gives an estimate of the mean fluctuation level. The introduction of a nonlinear stability

References

[1.21] E. Giovannozzi et al., Nucl. Fusion **44**, 226 (2004)

[1.22] S.V. Annibaldi et al., Nucl. Fusion **44**, 12 (2004)

[1.23] S. V. Annibaldi et al., *m=1 Magnetic island geometry*, presented at the Joint Varenna - Lausanne Int. Workshop on Theory of Fusion Plasmas (Varenna 2004)

[1.24] K.H. Burrell, Phys. Plasmas **4**, 1499 (1997); E. Mazzucato et al., Phys. Rev. Lett. **77**, 3145 (1996); E.J. Synakowski et al., ibid. **78**, 2972 (1997); H. Shirai et al., Phys. Plasmas **5**, 1712 (1998); G. Wang et al., ibid., p 1328

[1.25] T.S. Hahm, Plasma Phys. Control. Fusion **46**, A323 (2004)

[1.26] M.N. Rosenbluth and F.L. Hinton, Phys. Rev. Lett. **80**, 724 (1998)

[1.27] Z. Lin, Science **281**, 1835 (1998)

[1.28] L. Chen, Z. Lin and R. White, Phys. Plasmas **7**, 3129 (2000)

[1.29] Liu Chen et al., Nucl. Fusion **41**, 747 (2001)

[1.30] F. Zonca, R. White and L. Chen, Phys. Plasmas **11**, 2488 (2004)

[1.31] L. Chen, R. White and F. Zonca, Phys. Rev. Lett. **92**, 075004 (2004)

[1.32] E. Frieman and L. Chen, Phys. Fluids 25, 502 (1982)

[1.33] Z. Lin et al., Phys Rev Lett. **83**, 3645 (1999)

[1.34] Z. Lin et al., Phys Rev Lett. **88**, 195004 (2002); Phys. Plasmas **11**, 1099 (2004)

[1.35] Z. Lin, *Size scaling of turbulent transport in tokamak plasmas*, presented at the 19th IAEA Fusion Energy Conf. (Lyon 2002) IAEA 2002 TH1/1

[1.36] R. White et al., *Zonal flow dynamics and anomalous transport*, submitted to Phys. Plasmas

parameter in symbolic dynamics provides a useful means of analysing turbulence levels with the use of a single time sequence data stream, and gives a number that is similar to the Lyapunov exponent.

1.4.3 Role of nonlinear toroidal coupling in electron temperature gradient turbulence

Key findings from recent global gyrokinetic particle simulations [1.37] are that electron temperature gradient (ETG) instability saturates via nonlinear toroidal couplings and that turbulence streamers do not drive a large electron thermal transport, as expected from mixing length estimates. The nonlinear gyrokinetic theory confirms qualitatively key simulation results, among which, that the ETG spectral energy cascades to longer poloidal wavelengths [1.38] (fig.1.24). These analyses focus on toroidal ETG turbulence with a strong positive magnetic shear $s \approx 1$, of which flux-tube simulations predict large electron transport. The mechanism of instability saturation and electron transport could be very different in the weak shear region $|s| \ll 1$, where the dominant instability is a slab ETG [1.39]. The crucial role of low-η quasi-modes as mediators in nonlinear toroidal couplings is a possible explanation for the big difference in saturation and transport levels between flux-tube and global simulations. In fact, the mode number of low-η quasi-mode is $n^{1/2}$ [1.37,1.38]. Thus, proper radial resolution to describe their dependence imposes that the radial box size scale as $n^{1/2}\ \rho_e$, ρ_e being the electron Larmor radius. If quasi-mode dynamics is suppressed, then only parallel mode structure modification via the (0,1) mode and zonal flow dynamics can set the (much higher) saturation level of ETG turbulence. Finally, since all unstable eigenmodes participate in nonlinear toroidal couplings, using a small number of toroidal eigenmodes [1.40] may not accurately predict the saturation amplitude.

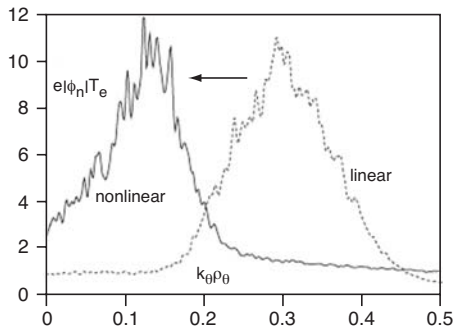

Fig. 1.24 - ETG fluctuation spectra in linear phase ($\times 10^5$, dotted) and at $t=20/\gamma_L$ after saturation ($\times 10^5$, solid), with γ_L the linear ETG growth rate

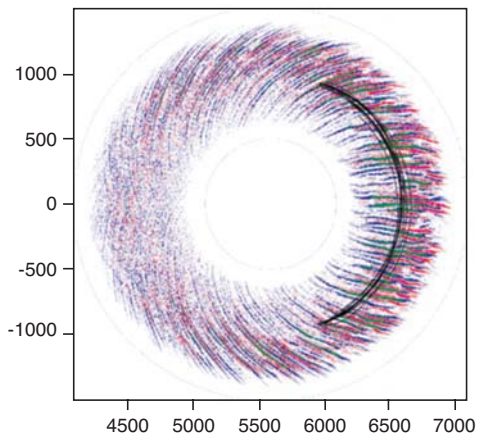

Fig. 1.25 - Poloidal contour plots of electrostatic potential at $t=20/\gamma_L$ after saturation. The poloidal projection of a typical electron orbit from saturation to $t=20/\gamma_L$ is plotted. The length unit is ρ_e

It should be noted that there is accumulating evidence from first-principle turbulence simulations that contradicts the heuristic mixing length rule, which underlies most of the existing transport models. A gradual transition from Bohm to gyro-Bohm scaling for ion transport driven by ITG turbulence was reported earlier [1.23,1.24,1.27], although the ITG eddies are isotropic. It has further been demonstrated that the scaling of electron transport driven by ETG turbulence is gyro-Bohm, even though the size of ETG streamers scales with the device size. The key to reconciling this obvious contradiction is that transport is diffusive (fig. 1.25) and driven by the local fluctuation intensity, rather than the eddy size. The deviation from gyro-Bohm scaling in ITG transport comes from the fact that the fluctuation intensity is driven by nonlocal effects such as turbulence spreading [1.23,1.24,1.27-1.29]. Meanwhile, ETG fluctuation intensity is determined by nonlinear toroidal coupling, which does not depend on the streamer (or system) size. In summary, global gyrokinetic particle simulation and nonlinear gyrokinetic theory find that ETG instability saturates via nonlinear toroidal couplings, which transfer energy successively from unstable modes to damped modes, preferably with longer poloidal

wavelengths (fig. 1.24). Electrostatic ETG turbulence is dominated by nonlinearly generated radial streamers. The length of the streamers scales with the device size and is much longer than the distance between mode rational surfaces or electron radial excursions. Both fluctuation intensity and transport level are independent of the streamer size. Simulations with realistic plasma parameters [1.38,1.39] find that the electron heat conductivity is much smaller than the experimental value, in contrast with the recent findings of flux-tube simulations that ETG turbulence is responsible for the anomalous electron thermal transport in fusion plasmas. Nonlinear toroidal couplings represent a new paradigm for the poloidal spectral cascade in plasma turbulence.

1.4.4 Effect of collisions on ITG-TEM and ETG turbulence in tokamaks

In collaboration with the Commissariat à l'Energie Atomique (CEA) Cadarache, France, stability analyses of electrostatic turbulence, i.e., ITG-driven and trapped electron modes (TEMs) and ETG-driven mode instabilities, have been carried out on FTU discharges by means of the numerical code KineZero [1.41]. The code, developed at Cadarache, computes the linear growth rate of the above-mentioned instabilities by solving the analytic dispersion relation obtained from gyrokinetic theory for non-collisional tokamak plasmas, by adopting the electrostatic approximation together with a ballooning ansatz for the eigenfunctions. However, collisionality is expected to play an important role in high-density plasmas, such as those of FTU as well as of pellet experiments in other fusion devices [1.42]. For this reason, corrections for finite collisionality have been included in a new version of the code. A Krook collision operator has been added to the Fokker-Planck equation, producing the following expression for the first-order perturbed distribution function:

$$\frac{\partial f_{1,s}}{\partial t} + \left[f_{1,s}, H_{0,s}\right] + \left[f_{0,s}, H_{1,s}\right] = -\nu_{fe}\left(f_{1,s} - \frac{n_{1,s}}{n_{0,s}} f_{0,s}\right)$$

where

$$\nu_{fe}\left(\varepsilon,\kappa\right) = \nu_{ei}\left(v_{the}/v\right)^3 Z_{eff}\left(\frac{1}{\varepsilon\left|2\kappa^2 - 1\right|}\frac{0.111\delta + 1.31}{11.79\delta + 1}\right)$$

and the Krook collision operator has been chosen in order to conserve particle number, but not momentum and energy [1.43,1.44]. An example of collision effects on the linear growth rates of ITG-TEM and ETG turbulence is shown in figures 1.26 and 1.27. The new version of the code was tested to verify its consistency with the previous version of KineZero in the limit of low collisionality ($\nu_{ei} \approx 0$). Also, the code outputs were compared with those of GS2, an electromagnetic code that solves the gyrokinetic equations in a flux tube. As previously done in [1.45], different runs were performed with the modified KineZero by changing both the collision frequency and the density gradient. The results obtained are in agreement with GS2 findings and show that the density gradient has a stabilising effect for ITG instabilities at high collisionality,

References

[1.37] Z. Lin, L. Chen and F. Zonca, *Electron temperature gradient turbulence*, submitted to Phys. Rev. Lett.

[1.38] Z. Lin, L. Chen and F. Zonca, *Role of nonlinear toroidal coupling in electron temperature gradient turbulence*, submitted to Phys. Plasmas

[1.39] Y. Idomura and M. Wakatani, Phys. Plasmas **7**, 3551 (2000)

[1.40] F. Jenko et al., Phys. Plasmas **7**, 1904 (2000); W. Dorland et al., Phys. Rev. Lett. **85**, 5579 (2000)

[1.41] J. Candy et al., Phys. Plasmas **11**, L25 (2004); Phys. Rev. Lett. **91**, 045001 (2003)

[1.42] C. Bourdelle et al., Nucl. Fusion **42**, 892 (2002)

[1.43] M. Romanelli, C. Bourdelle and W. Dorland, Phys. Plasmas **11**, 3845 (2004)

[1.44 G. Rewoldt, W. M. Tang and E. A. Frieman, Phys. Fluids 20, 402 (1977)

[1.45] M. Kotschenreuther, G. Rewoldt and W.M. Tang, Comp. Phys. Comm. **88**, 128 (1995)

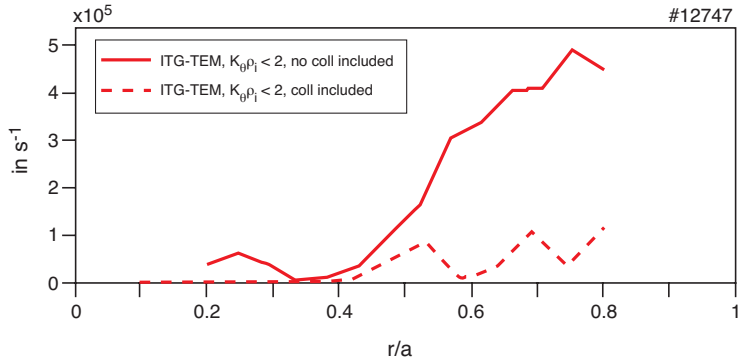

Fig. 1.26 - Maximum linear growth rate computed by KineZero for ITG-TEM instabilities (FTU pulse #12747 at t=0.8 s)

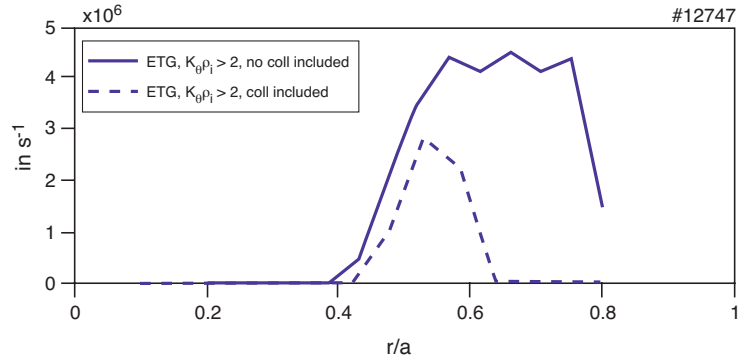

Fig. 1.27 - Maximum linear growth rate computed by KineZero for ETG instabilities (FTU pulse #12747 at t=0.8 s)

whereas at low collisionality the effect is the opposite. The advantage of using the modified version of KineZero is that of having a quick, reliable tool for studying electrostatic instabilities in a tokamak, whereas other codes, such as GS2, require more computer resources and CPU time to run.

1.4.5 Transport studies on FTU

Transport and confinement on FTU have been extensively studied. A set of validated transport codes (JETTO, EVITA and CRONOS) was used to study the transport properties of a variety of discharges, with particular emphasis on density scan, pellet-fuelled and radiofrequency-heated discharges. It was shown [1.46] that electron transport is the main heat loss channel in low-density Ohmic discharges [linear Ohmic confinement (LOC)], with electron thermal conductivity values two orders of magnitude larger than the values of neoclassical conductivity. By increasing the density, a region of saturated Ohmic confinement is approached, where the electron heat conductivity decreases down to the ion neoclassical value, but the ion heat conductivity remains between three and six times the neoclassical transport level. It was recognised that the improved confinement in pellet-fuelled discharges is due to the ion heat conductivity decreasing down to its neoclassical value, whereas the electron heat conductivity remains the same order of magnitude. The study of micro-turbulence in FTU pellet-fuelled discharges [1.43] indicates the stabilisation of ITG-TEM and ETG instabilities, mainly due to the change in the density profile. It was shown that this stabilisation is essentially allowed by the high collisionality regime characterising FTU discharges (T_e=keV, $n_{e0}=1\times10^{21}$ m^{-3}). The possible stabilising effect due to electromagnetic modes (namely Alfvén ion temperature gradient) was assessed, and it was found that FTU pellet fuelled discharges lie in a region where the ballooning alpha parameter is about half the critical value, and the possibility of further stabilising small-scale turbulence by increasing the pressure gradient was indicated. Electron ITBs are now routinely achieved on FTU with ECRH and LH heating. JETTO was used as a predictive tool to study the time evolution of the current density profile during the current ramp up phase in order to optimise the LH heating and current drive schemes. The time evolution of temperatures is well described by the Bohm-gyro-Bohm shear-dependent transport model [1.47]. The study of e-ITB formation in terms of turbulence suppression and change in the transport channels is the subject of ongoing research activities.

1.4.6 Particle transport studies in FTU

The mechanisms underlying particle transport and the formation of peaked density profiles have been addressed. Clear evidence of anomalous peaking of the density has been given by the experiments carried

out on Tore Supra where the main neoclassical drive (Ware pinch) was eliminated by performing long-lasting LH current drive discharges. The residual particle pinch due to turbulence was measured in terms of the temperature gradient (thermodiffusion) and the safety-factor gradient (turbulence equipartition) [1.48]. Analogous experiments were carried out on FTU at higher densities (ITER-relevant) and higher magnetic field. Analysis of zero loop voltage FTU discharges has already indicated the presence of an anomalous pinch, which scales with the gradients of temperature and safety factor. Further analyses and modelling of the new experimental data are in progress.

1.4.7 Analysis and modelling of LHW propagation in toroidal plasmas

A new approach for modelling LHWs in plasmas has been successfully applied to JET experiments in the strong ITB regime [1.49]. The approach is characterised by including, in the ray-tracing quasi-linear analysis, the spectral broadening induced by the LH parametric instability at the plasma edge [1.50]. The modelling of such a nonlinear process leads to a much broader spectrum than the usual one calculated by linear models, which propagates towards the plasma core. The formation and localisation of the ITB in selected JET discharges have been described successfully by using this approach.

At the same time, the LH full wave equation in the electrostatic approximation and in general magnetic field equilibria, which goes beyond the usual Wenzel, Kramer, Brillouin (WKB) approximation (ray-tracing equations), was numerically integrated when the magnetic equilibrium reduces to a system of circular and concentric magnetic surfaces. This work was done in view of comparing the full numerical integration with a new analytical approach, which treats the wave equation by a multiple spatial scale method based on the Poisson summation formula [1.51,1.52].

In applying this formalism, in fact, the starting equation for the scalar potential in the cold plasma limit reduces to two nested 1D equations: the first governs the wave structure along the magnetic field lines; the second describes the slow radial dependence of the wave envelope, for which the usual WKB asymptotic technique is applied.

The numerical solution of the full 2D wave equation was obtained by using a spectral approach based on Fourier analysis of the scalar potential in the periodic variables θ and ϕ. The starting partial differential equation (PDE) for the potential is replaced by a system of coupled ordinary differential equations in r. The solution of the set of coupled equations requires the use of non-standard methods (shooting methods) because of difficulties in properly fixing the correct boundary conditions and also to avoid consuming a large amount of computational memory. The complete solution can be finally obtained by numerical methods based on the fast Fourier transform. Well-known characteristic behaviour of LHW propagation, such as resonance cones of a Gaussian beam in a cold plasma etc., is studied as benchmarks of the numerical solution.

1.4.8 Modelling of the ICRH experiment on JET

The aim of this modelling study is to first evaluate the main features of the proposed ion cyclotron resonance heating (ICRH) experiment and then to perform a detailed analysis of the experimental discharges. The proposed experiment

References

[1.46] B. Esposito et al., Plasma Phys. Control. Fusion **46**, 1793 (2004)

[1.47] G. Vlad et al., Nucl. Fusion **38**, 557 (1998)

[1.48] X. Garbet et al., Phys. Rev. Lett. **91**, 035001 (2003)

[1.49] R. Cesario et al., Phys. Rev. Lett. **92**, 175002 (2004)

[1.50] R. Cesario et al., *Spectral broadening of lower hybrid waves produced by parametric instability in current drive experiments of tokamak plasmas*, submitted to Nucl. Fusion

[1.51] A. Cardinali and F. Zonca, Phys. Plasmas **10**, 4199 (2003)

[1.52] A. Cardinali and F. Zonca, *Analytical and numerical study of the lower-hybrid-relevant wave equation in a toroidal plasma*, presented at the Sherwood Theory Conf. (Missoula 2004)

concerns essentially the possibility of obtaining ITBs on both the ion and the electron species with only the use of the ICRH system in an ion-heating scheme and without the help of neutral beam injection (external momentum input) [1.53]. In this context, an ITB regime on JET was obtained by using 6 MW of ICRH in the minority heating scheme [1.54].

The minority species involved is ^{3}He. The scheme should act at the fundamental cyclotron harmonic of the minority species ($\omega=\Omega_{cm}$) located near the plasma centre, while either the fundamental or the first harmonic of the majority (($\omega=\Omega_{cM}$) or ($\omega=2\Omega_{cM}$) is outside the plasma. This is the so-called isolated case. Cyclotron resonance heating of the minority is very efficient, the reason being that the fast wave polarization is essentially determined by the majority species alone, while damping is due mainly to the resonant minority ions (minority heating regime). If the minority concentration increases too much, the screening due to the rotating electric field is no longer negligible and cyclotron damping drastically decreases, entering the "mode conversion regime". When programming an ICRH heating experiment, it is important to establish plasma and antenna parameters that fit the goals well. In the ICRH minority heating experiment on JET, antenna and plasma parameters are chosen by maximising the power coupled to the plasma, without dealing with edge cut-offs on the low field side ($n_{||}=r$), and by choosing the right minority concentration in order to avoid the mode conversion regime.

The characteristics of the codes used to plan and model the ICRH experiment are reported below:

(i) A code which solves the cold plasma electromagnetic dispersion relation in slab geometry so as to make the dispersion characteristics of the experiment clear. Then, it is possible to establish the range of variation in the main parameters, such as the power spectrum $n_{||}$ vs. the plasma density profiles, in order to assess accessibility conditions, such as the minority concentration, in a plasma with two ion species (or more) and the localisation of the ion-ion resonance (and the associated cut-off), which turns out to be very close to the ion cyclotron resonance of the minority species, etc.

(ii) A code which solves the warm plasma electromagnetic dispersion relation in the complex space of the wavenumber, in order to clarify the role of wave damping on the minority species, and the effects of the plasma parameters (minority concentration, ion and electron temperature, parallel wave-numbers involved) on the transition to the mode conversion regime. The use of this code should also provide the power deposition profiles and power damping rate for the whole launched spectrum.

(iii) A 1D ray-tracing code in cylindrical geometry to take into account, at the lowest order, the geometry of the tokamak plasma. The code uses the warm plasma electromagnetic dispersion relation at point (ii).

(iv) Eventually, a 2D complex ray-tracing code in tokamak geometry to take realistic geometry into account. This code is based on a complex full electromagnetic dispersion relation and complex integration of the trajectories.

(v) A 1D full-wave code FELICE, which gives the linear distribution of the wave power on the ion and electron species, which accounts correctly for the electron Landau damping in the fast-wave branch and in the IBW branch, as well as for the realistic antenna-plasma coupling, calculating the whole effect of the power spectrum on the various species.

(vi) A 2D full-wave code TORIC, with the same characteristics as the 1D FELICE code, but including the real plasma geometry (in the flux surface coordinate system).

(vii) A 2D full-wave code Fokker-Planck/TORIC, which does the same as (vi) but includes the evolution of the 2D distribution function for ions and electrons.

1.4.9 Geometry of the m=1 magnetic island

The shape of an m=1 magnetic island, as observed in FTU, has been realistically reconstructed theoretically. Experimental results lead one to consider a cylindrical equilibrium. The plasma cross section is divided into three radial areas: an internal area, from the plasma centre up to $r=r_s-\Delta r$, an external one, from $r=r_s+\Delta r$ up to the plasma edge (r_s is the radius of the q=1 magnetic surface and Δr is finite), and a

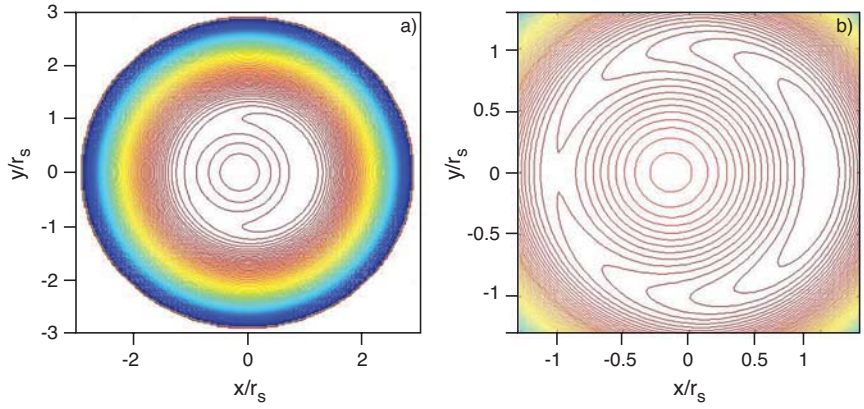

Fig. 1.28 - Helical magnetic flux surface sections in the presence of an m=1 magnetic island, obtained with the model. a) Full plasma section. b) Enlargement

toroidal annulus of $2\Delta r$ width, centred about r_s. In the internal and external regions, one writes a helical modification of the Grad-Shafranov equation, which is further linearised by considering the helical magnetic flux as being composed of a dominant axisymmetric part plus a small single helicity perturbation. A numerical approach is used to find this perturbation.

In the toroidal annulus, centred about the q=1 surface, the equilibrium condition is rewritten, using r as radial coordinate, since the radial derivative of the helical flux vanishes on the q=1 surface, leading to an infinite Jacobian when using flux coordinates. This equilibrium equation is solved numerically, keeping the full nonlinearity. The three solutions are then matched to finally obtain the complete shape of the helical flux surface sections (fig. 1.28), which is comparable with the experimental observations. Studies indicate that nonlinearities cannot be neglected in the island geometry and that considering finite toroidicity would include next-order corrections in the results but is not essential for reproducing the fundamental shape of the island.

1.4.10 Avalanches in fusion product transport

Simulation results indicate that, above the threshold for the onset of resonant EPMs, strong fast ion transport occurs in avalanches [1.55] (fig. 1.29). Such strong transport events occur in time scales of a few inverse linear growth rates (generally 100-200 Alfvén times) and have a ballistic character [1.56] that basically differentiates them from the diffusive and local nature of weak transport. Meanwhile, numerical simulations have demonstrated that Alfvén cascades in JET [1.57] are consistent with both weak and strong fast ion transport [1.58]. Recently, experimental observations at the JT-60U tokamak have also confirmed macroscopic and rapid (in the sense discussed above) energetic particle radial redistributions in connection with the so-called abrupt large amplitude events [1.59]. Therefore, it is crucial to theoretically assess the potential impact of fusion product avalanches on

References

[1.53] A. Cardinali, *Modellizzazione di esperimenti alla frequenza ionico ciclotronica sul tokamak JET (Joint European Torus) e FTU (Frascati Tokamak Upgrade)*, presented at the XC Congresso Nazionale della Società Italiana di Fisica (Brescia 2004)

[1.54] F. Crisanti et al., *Experimental evidence of ion internal transport barrier without injection of external momentum input*, presented at the Transport Task Force Meeting (Varenna 2004)

[1.55] F. Zonca et al., *Collective effects and self-consistent energetic particle dynamics in advanced tokamaks*, Paper TH/4-4, presented at the 19th IAEA Fusion Energy Conference, Lyon, France, Oct. 14-19 (2002)

[1.56] R.B. White et al., Phys. Fluids **26**, 2958 (1983)

[1.57] S.E. Sharapov et al., Phys. Lett. **A289**, 127 (2001)

[1.58] F. Zonca et al., Phys. Plasmas **9**, 4939 (2002)

[1.59] K. Shinohara et al., Nucl. Fusion **41**, 603 (2001)

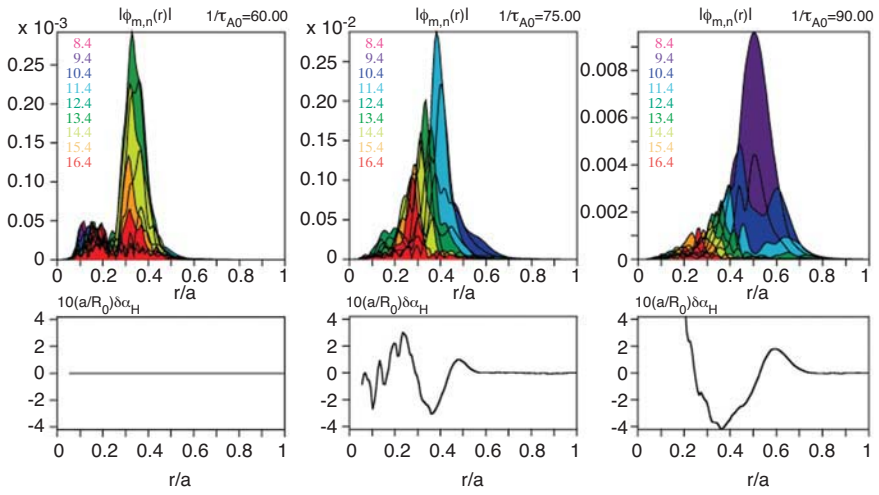

Fig. 1.29 - Time evolution of the EPM radial structure, decomposed in poloidal Fourier harmonics. Here $\tau_{A0}=R_0/v_{A0}$, with R_0 the tokamak major radius and v_{A0} the on-axis Alfvén speed. The toroidal mode number is n=4. The rescaled nonlinear modification $10/(aR_0/\delta\alpha_H)$ of the energetic particle $\alpha_H=-R_0q^2(d\beta_H/dr)$ is also shown [1.35], with a the tokamak minor radius

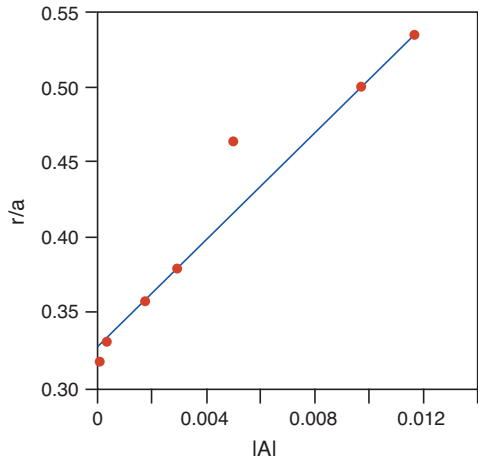

Fig. 1.30 - Radial position of the maximum EPM amplitude vs. the peak amplitude itself, during the convective amplification process

burning plasma operation in the perspective of direct comparisons of those predictions with experimental evidence. The change in nonlinear EPM dynamics that accompanies the transition from weak to strong energetic ion transport has been studied. It has been demonstrated that the nonlinear threshold in fast ion energy density for the onset of avalanches is close to the linear EPM excitation threshold. This phenomenology is strictly related to the resonant character of the modes, which tend to be radially localised where the drive is strongest [1.60,1.61]. When the nonlinear threshold is exceeded, the EPM envelope propagates radially for two reasons: the radial dispersiveness of the mode and the rapid redistribution of the energetic particle source. These two effects can be viewed as manifestations of linear and nonlinear EPM radial group velocities, respectively. As it propagates, the EPM radial envelope is convectively amplified due to resonant wave-particle interactions (fig. 1.30), which are responsible for the secular motion of the unstable front, too, and, ultimately, of the avalanching process [1.62]. After the convective loss phase, during which the nonlinear EPM mode structure is displaced outwards, fast ion transport continues due to diffusive processes. The theoretical analyses are the basis for consistency analyses of the operation scenarios of the proposed burning plasma experiments.

1.4.11 Alfvénic instabilities in ITER scenarios

The work on Alfvénic instabilities in ITER scenarios was done in collaboration with the Association Euratom-CEA, CEA/DSM/DRFC Cadarache, France. The stability of the proposed ITER scenarios with respect to Alfvénic fluctuations driven by fusion-produced alpha particles has been analysed by means of particle-in-cell simulations. Three scenarios have been considered: SC2, characterised by a monotonic q profile; the reversed-shear SC4 scenario; and a flat q-profile "hybrid" scenario, SCH (here q is the safety factor). All these cases were found to be unstable, though the mode growth rates are quite small. For all the scenarios, the most unstable modes correspond to low toroidal numbers (n=4 in the SCH case, n=2 in the other two cases). They are localised in low-shear regions (the inner portion of the plasma for SC2

and SCH, mid-radius for SC4), where they can easily avoid the damping interaction with the Alfvén continuum. A common feature of these modes is represented by their MHD-like nature: in the limit of zero drive, they smoothly connect to MHD quasi-marginally-stable modes. The radial localisation of the modes almost coincides with that of the maximum drive for SC2 and SC4, but not for SCH. In SCH, the mode grows around an inner flux surface with respect to the $\alpha_H=-R_0q^2\beta_H'$ peak (here R_0 is the major radius of the torus, β_H is the ratio between alpha-particle and magnetic pressure and prime denotes radial derivative). The fact that the mode can grow even though the drive is quite small is not surprising, because of its MHD nature (it exists even in the absence of energetic particles); at the same time, it justifies the very low growth rates obtained in this case.

If the drive is artificially increased above that of the reference scenario (preserving its normalised radial profile), apart from the obvious increase in the growth rates of these MHD-like modes, destabilisation of fast-growing EPMs can occur in the SCH case around the maximum drive radial position. At that position only heavily damped Alfvén oscillations can take place in the MHD limit. Energetic particle modes appear only if the energetic-particle drive exceeds a certain threshold. In the SCH case, this threshold corresponds to an alpha-particle energy content greater than the reference value by a factor of $\approx$1.6. This should not be considered unrealistically high, because at least two factors can cause an underestimation of the fast-ion energy density: first, the strong dependence of the fusion-produced alpha-particle density on the electron and bulk-ion temperatures, along with the intrinsic uncertainties of transport models (a 60% error in β_H can be accounted for by a 15% error in bulk-plasma temperatures); second, the fact that equilibrium profiles used in the simulations neglect the concurrent drive associated with the energetic particles produced by additional heating.

Concerning the destabilising mechanisms, it has been shown that $n\leq 8$ EPMs are driven unstable mainly by the resonance with trapped energetic particles: indeed, they disappear if the mirroring term in the energetic-particle parallel dynamics is artificially removed. The MHD-like modes are apparently less sensitive to a specific resonance and, consistent with their character, they do not discriminate between trapped and transit particle dynamics.

Investigation of the system nonlinear dynamics has shown that the effects on the alpha-particle confinement at the reference drive values are very small for SC2 and SCH. For the SC4 scenario, some broadening of the alpha-particle pressure profile is observed, indicating that the scenario itself has a certain level of inconsistency. Simulations performed with increasing drive intensity show that a strong flattening of the alpha-particle pressure profile can occur in the inner plasma region for SC2, while the global confinement of such particles is not significantly affected. The SC4 case presents effects that are more pronounced in the outer portion of the discharge because of the outer localisation of the modes, with less impact on the on-axis pressure value. Further diffusion due to saturated fields leads to particle losses even for relatively moderate drive increase. In the SCH scenario, no significant consequences are observed below the EPM threshold. If such a threshold is exceeded, the effects on the alpha-particle pressure are similar to those in the SC4 case, but are more limited for a given growth rate.

On the basis of these results, it is possible to conclude that all the considered ITER scenarios deserve further investigation in order to assess their consistency with Alfvén mode dynamics. This is apparent for the SC4 case, which presents modifications of the alpha-particle pressure profile even at the reference value. For the other two cases, more accurate analyses are needed due to the difficulties in predicting exactly the energetic-particle energy content and, hence, in excluding that the system be characterised by significantly more unstable regimes.

References

[1.60] F. Zonca and L. Chen, Phys. Plasmas **3**, 323 (1996)

[1.61] F. Zonca and L. Chen, Phys. Plasmas **7**, 4600 (2000)

[1.62] F. Zonca et al., *Consistency of proposed burning plasma scenarios with alpha particle transport induced by Alfvénic instabilities*, presented at the 8th IAEA Technical Meeting on Energetic Particles in Magnetic Conf. Systems (San Diego 2003)

1.4.12 Grid-based distributed particle-in-cell simulation

The issue of distributing parallel computation among the Globus machines of a grid environment in the case of a particle-in-cell code has been studied in collaboration with the Second University of Naples. A cluster of workstations was configured as a distributed system of four single-node symmetric multiprocessor (SMP) Globus machines, as a lowest-order approximation of a more complex, geographically-distributed, heterogeneous grid. Installing the MPICH-G2 library and the Intel FORTRAN compiler on the cluster allowed porting of a parallel version of the application, based on the hierarchical integration of the message-passing interface (MPI) and OpenMP, originally developed for generic (non-grid) clusters of SMP nodes. It was then possible to compare the performance obtained on the grid environment with that obtained with the simple cluster of SMP nodes (same hardware). It was found that although the parallelization efficiency is slightly reduced it still remains at a fairly high level.

Although integration of the Globus toolkit and Intel compiler was not a straightforward task, the related effort was valuable, as the Intel compiler allows one to use the OpenMP facility and fully exploit the SMP architecture of each node. Replacing OpenMP programming with the execution of as many MPI processes as the processors owned by each node yields indeed lower efficiency values.

Finally, the time offsets due to submitting the request to the gatekeepers, activating the processes and releasing the resources, although scaling with the number of Globus machines, appear to be negligible compared to realistic-simulation elapsed times.

These conclusions are partly affected, of course, by the almost-ideal character of the grid environment considered (close, homogeneous, dedicated nodes): real grid porting of the same application, which will be the subject of future work, could turn out to be much less efficient. Nonetheless, such porting would maintain its relevance with respect to the task of increasing memory resources (and, then, the achievable simulation size).

1.5.1 Introduction

ENEA's participation in the JET experimental (C8 and C14) campaigns continued with one task force leader and two deputies in charge of programme preparation and with the execution of activities related to Task Forces S2 (Advanced Tokamak Scenario), S1 (H-mode), D (Diagnostics), M (Magnetics) and H (Heating), DT (Deuterium–Tritium).

Campaigns C12b, C13 and C14 were carried out from 7 January to 5 March 2004. A general review meeting (GRM) was held in September 2004 to discuss the JET-related activities of the ENEA Association laboratories (ENEA Frascati, Institute of Plasma Physics of CNR Milan, CNR-RFX Padua) and the universities (CREATE Consortium, Turin Polytechnic). It was agreed to focus the activities of the ENEA Association on just a few headlines of the JET programme so as to increase the efficiency of the participation.

1.5.2 ENEA Frascati experiments in C14

Development of dominant ICRH in electron ITB scenario. As described in the 2003 Progress Report, ion internal transport barriers (ITBs) were obtained with low torque injection by heating the ions with a high (5-8%) ^{3}He concentration, ICRH minority scheme on pure LHCD electron ITBs. This suggests that, in addition to the ExB shearing rate, other turbulence stabilising mechanisms are present. Typical discharge parameters (shot #62607) were B_T=3.45 T, I_P=2.5 MA, $<n_e>$~2×10^{19} m^{-3}, P_{LH}=2 MW, P_{ICRH}=6 MW at 37 MHz in the ^{3}He minority heating scheme. In these conditions an ion ITB was generated in the presence of an electron ITB with a q profile with flat shear (1/q (dq/dr)). The main traces related to shot #62607 are shown in figure 1.31.

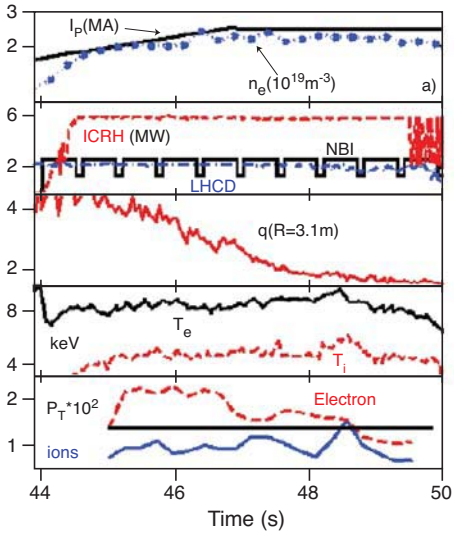

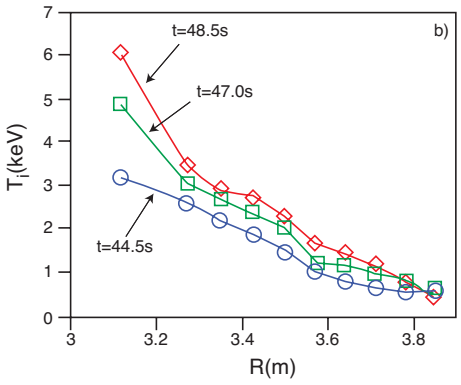

Fig. 1.31 - a) Main traces of shot #62607. NBI power was used for the measurements of charge exchange recombination spectroscopy and motional Stark effect. b) The radial profile of the ion temperature evolution. The gradient of T_i increases at t=48.5 s

An ion ITB was obtained for lower toroidal plasma rotation values than those usually obtained in ITB discharges with dominant neutral beam injection (NBI) heating. Figure 1.32 shows the time evolution of plasma rotation velocity for shot #62607.

The confinement properties of the discharge can be appreciated in figure 1.33, which shows the ion diffusivity and the ExB shearing rate (ω_S) time evolution, together with two evaluations of the ITG growth rate. The shearing rate for shot #53521 is also reported for comparison.

Hybrid scenario with dominant electron heating. Scenarios dominated by radio-frequency (rf) heating were obtained at B_t=3.2 T, I_P=2.6 MA, q_{95}=3.8 (with q_{95} the safety factor at 95% of the poloidal flux) , achieving a quality factor of H_{89N}/q_{95}^2~0.2 (H_{89N} is the enhancement factor over the L-mode confinement scaling), with T_i~0.8 T_e, very low edge pedestal and low edge localised mode (ELM) activity (#62789). Motional Stark effect measurement of the safety factor spatial profile shows a wide low magnetic shear (q~1) area extending to half radius. Magnetohydrodynamic events include toroidal Alfvén eigenmodes, neoclassical tearing modes (3/2 mode saturates at low amplitude, full island width 0.05r/a) and n=1 modes (with slow temperature oscillations which do not affect global performance). Scans

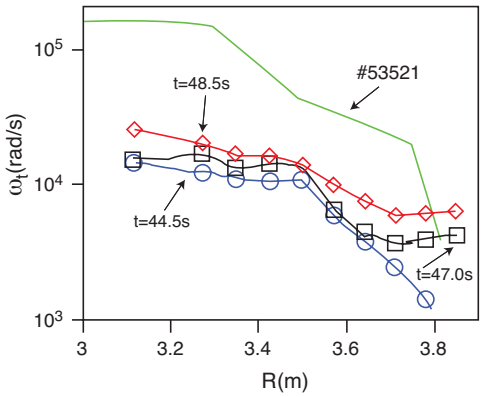

Fig. 1.32 - Spatial profile of toroidal rotation for shot #62607, compared with the profile measured in a JET ITB with dominant NBI heating (shot #53521, with I_P=2 MA, P_{NBI}=14.6 MW, P_{LH}=2.6 MW, P_{ICRH}=4 MW)

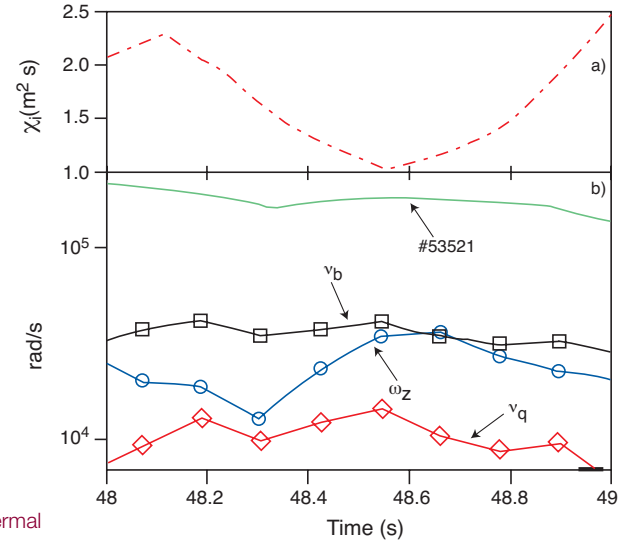

Fig. 1.33 - Transport properties of shot #62607: a) ion thermal diffusivity; b) ExB shearing rate

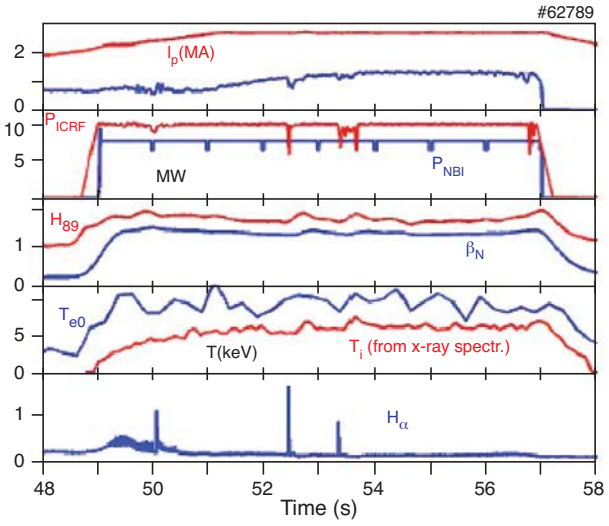

Fig.1.34 - Main traces of rf-dominated hybrid scenario (shot #62789). The low ELM activity can be noted (see measurement of H_α emission). The ion temperature is measured by x-ray crystal spectroscopy at r/a=0.4

in plasma current (I_P~1.9-2.6 MA) (at B_t=3.2 T, and P_{tot}~16-20 MW) suggest that H_{89N} is not dependent on q_{95}, and that the quality factor H_{89N}/q_{95}^2 seems limited by power, and not by MHD. The maximum normalised beta achieved is still not very high (β_N=1.5), as a consequence of the relatively low additional heating available. In this scenario the shear was flat and q_0 close to one; however, unlike the standard scenario, fishbone activity was missing and mild sawtooth (with a very long crash time) activity was often present. The main traces related to shot #62789 are shown in figure 1.34.

Slowly growing n=1 internal kink modes have been identified as the main core MHD activity in a hybrid regime with strong electron heating. The effect of these modes on plasma performance has been studied and their interaction with Alfvén eigenmodes, neoclassical tearing modes and fishbones has been documented.

Dependence of configuration on neutral-point perturbation. Plasma disturbances such as radiative collapse or giant ELMs induce eddy currents in the passive structures. The currents interact with the plasma, causing perturbation in the plasma position. Since the n=0 mode is unstable for elongated plasmas, the vertical plasma position will evolve exponentially in a preferential direction (i.e., up or down). The initial excitation of the unstable mode, and hence the direction of movement, will depend in general on the position of the plasma before the disturbance. In fact the neutral point (NP) is defined as the position where the unstable mode is not excited by a given perturbation. The existence of a NP has been clearly demonstrated for plasma disruptions following radiative collapses in JET. The same investigation was performed for vertical instabilities triggered by ELMs and, contrary to the previous case (i.e., radiative collapse), no NP was found.

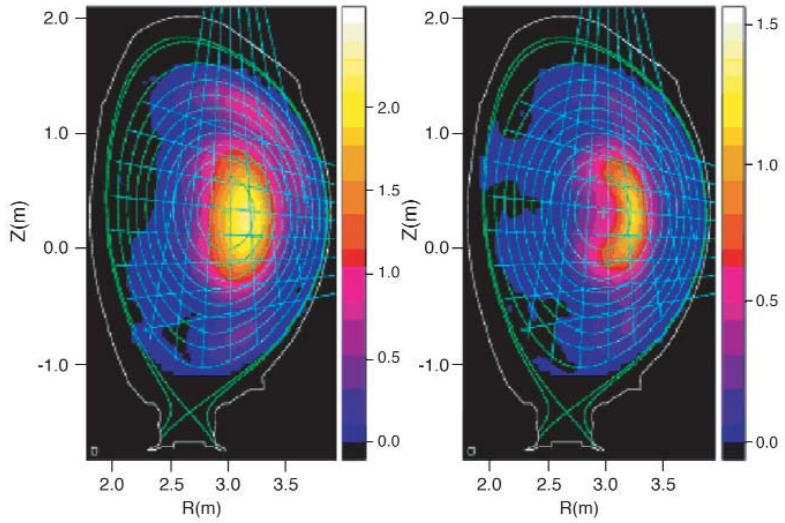

Fig. 1.35 - Tomographic reconstruction of fast D ions (left) and fast alpha particles (right) measured simultaneously by the horizontal and vertical gamma cameras during alpha-particle simulation experiments. The fast D ions result from parasitic ion cyclotron resonance frequency absorption

Extreme shape controller. The extreme shape controller (XSC) is designed to keep the plasma shape (high triangularity and/or elongation) constant while varying the beta poloidal and internal inductance. This tool has a certain relevance for ITER because it will work at high values of triangularity and elongation. A linearised plasma model approach was used to

design the XSC for JET single-null configurations. The plasma modelling tools (CREATE-L and CREATE-NL codes) have been set up on the JET configuration. The codes include an equivalent axisymmetric model of the iron core and also take into account the eddy currents induced in the passive structures. The input quantities are the poloidal field circuit currents (or voltages) and a number of parameters related to the plasma current density profile. The output quantities include the signals provided by the magnetic diagnostic system for measuring the JET plasma current and shape. The model was validated with closed loop simulations, which provided a reliable starting point for the design and assessment of a new current, shape and position control system for JET. The model also allowed a better understanding of a set of experiments devoted to detecting the neutral point when density limit disruptions occur and when the strike points jump in correspondence to ELMs. The shape is accurately described by 32 plasma-wall gaps, the positions of the inner and outer separatrix strike points and the radial/vertical location of the X-point. As only a limited set of actuators was available, a singular value decomposition was used to identify the principal directions of the algebraic mapping between coil currents and geometrical descriptors. The principal directions identify eight linear combinations of currents, each one influencing one linear combination of geometrical descriptors. In this way the original multivariable control problem can be solved by using a set of separate proportional integrative derivative (PID) controllers. The XSC was run on JET in a set of dedicated experiments and then successfully used in a number of JET sessions: in shot #61995 the desired high triangularity was kept within a 2–cm tolerance, even in the presence of wide excursions of l_p and l_i (1-1.5).

Confinement of fast ^{4}He ions: gamma-ray and neutron diagnostics. The gamma-ray spectroscopy diagnostic for measuring the fast-ion distribution function was exploited during the Alpha Physics Experiment. The technique is based on the detection of gamma rays from nuclear reactions which have a high energy threshold for alphas (E>1.7 MeV) and deuterium (E>0.8 MeV). The gamma rays are sufficiently separated in energy (4.44 MeV for alphas, 3.01 MeV for deuterium) to allow good discrimination between the alphas and the deuterium, thus allowing simultaneous measurement (fig. 1.35). The confinement of the fast alphas could be directly observed in various plasma regimes by analysing neutron/gamma measurements.

The trace tritium experimental (TTE) campaign continued [1.63,1.64] with tritium transport studies, investigation of the influence of fast particles on the plasma, new heating scenarios and ITER-relevant developments in burning plasma diagnostics [1.65-1.67].

Neutron spatial distribution. The neutron emission profile diagnostic played a key role in providing information on the tritium transport features in different plasma scenarios [1.68]. In the experiments on new heating schemes and fast particle physics, clear evidence of spatial asymmetries in the neutron emission was observed in the vertical camera measurements. In

References

[1.63] D. Stork et al., *Overview of transport, fast particle and heating and current drive physics using tritium in JET plasmas*, presented at the 20th IAEA Int. Conf. on Fusion Energy (Vilamoura 2004), to appear in Nuclear Fusion

[1.64] T.T.C. Jones et al., *Technical and scientific aspects of the JET trace-tritium experimental campaign*, presented at the 7th Conf. on Tritium Science and Technology (Baden Baden 2004)

[1.65] S. Popovichev et al., *Performance of neutron measurements during trace tritium experiments on JET*, presented at the 31st Eur. Physics Society Conf. on Plasma Physics (London 2004)

[1.66] L. Bertalot et al., *ITER-relevant developments in neutron diagnostics during the JET trace tritium campaign*, presented at the 23rd Symp. on Fusion Technology (Venice 2004)

[1.67] A. Murari et al., *New developments in JET neutron, alpha particle and fuel mixture diagnostics with potential relevance to ITER*, presented at the 20th IAEA Int. Conf. on Fusion Energy (Vilamoura 2004), to appear in Nuclear Fusion

[1.68] K-D. Zastrow et al., Plasma Phys. Control. Fusion **46**, B255 (2004)

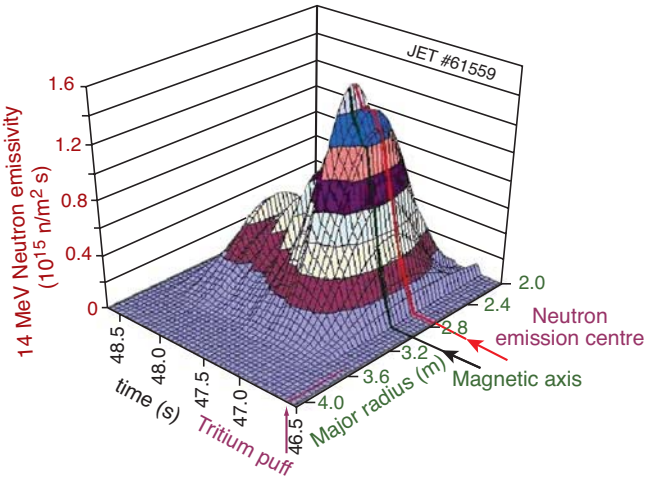

Fig. 1.36 - 14-MeV neutron profile measured during ICRH tritium fundamental heating showing that the neutron emission centre is shifted to the high-field side with respect to the magnetic axis

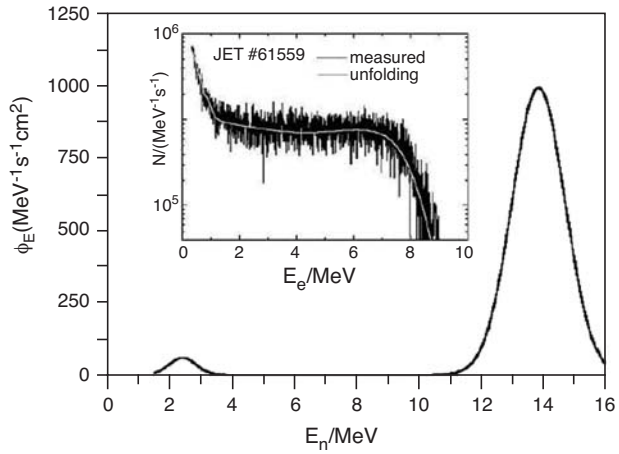

Fig. 1.37 - Neutron spectrum determined experimentally with the PTB-NE213 system (JET shot #61559, ICRH fundamental tritium heating). Insert: measured pulse height spectrum and unfolding of the neutron spectrum with the response functions

the tritium fundamental rf heating scenario [1.69] (a possible ITER heating scheme), the 14-MeV neutron emission axis is not located along the magnetic axis but is shifted towards the high-field side near the tritium cyclotron resonance layer, located at R=2.55 m (fig. 1.36).

Off- and on-axis tritium beams in strong reversed shear plasmas were used as fast probe particles for studying the effect of current holes on fast-particle confinement. An outward or inward displacement of the neutron emission from the magnetic axis was also detected for on/off-axis beam injection, respectively, indicating the effect of orbit distortion due to the low poloidal field in such plasmas [1.70].

Gamma diagnostics. During the TTE, the slowing down of fusion-born alphas was measured for the first time [1.71] by means of the gamma emission due to the nuclear reaction ^{9}Be(α,nγ)^{12}C. Classical estimates of alpha confinement were confirmed, but some advanced scenarios with a current hole show significant losses of the fusion alphas. These experimental results can be reconciled with the theory of classical collisions if the region of almost zero current, and therefore negligible poloidal field, is properly taken into account. For magnetic configurations with a current hole, therefore, gamma-ray spectroscopy confirms the evidence of enhanced collisional losses, implying a reduction in fast-particle confinement, as indicated by the neutron profile monitor.

Moreover, during the alpha physics experiment, the energy distributions of accelerated ^{4}He ions and fast deuterons in ^{4}He plasmas were determined by means of gamma and neutron spectroscopic measurements. Two-dimensional imaging of the gamma radiation, obtained with the CsI(Tl) detectors of the neutron profile monitor, provides information on the spatial distribution of both accelerated ^{4}He ions and fast deuterons [1.72].

Neutron energy distribution. Compact broadband neutron spectrometers based on scintillators with pulse-shape discrimination features have been considered as possible diagnostic systems for ITER [1.73].

In collaboration with the Physikalisch-Technische Bundesanstalt (Germany), measurements with a NE213 liquid scintillator were successfully carried out during the TTE, achieving energy resolutions of $\Delta E/E<4\%$ and $\Delta E/E<2\%$, at neutron energies of 2.5 and 14 MeV, respectively. New data-analysis techniques based

on Bayesian methods, L-curve techniques and maximum entropy unfolding have been developed. Pulse–height spectra were acquired from different plasma heating scenarios ([1.74] and (fig. 1.37).

The digital pulse-shape discrimination system developed at ENEA Frascati (see 2003 Progress Report) for neutron counting and pulse-height gamma and neutron spectroscopy was successfully implemented during the TTE with a NE213 liquid scintillator at high count rates (MHz range) [1.75,1.76].

1.5.3 General Review Meeting of ENEA Association and participation in 2005-6 JET campaigns

At the General Review Meeting in September 2004, participation in the 2003-4 JET campaigns was discussed in detail and general guidelines were established for participating in the 2005-6 campaigns. The ENEA Association suggested focussing the activities on a few headlines.

Consequently, the proposals will be organised as follows:

1. ITER-relevant ITB scenario at high bootstrap fraction (f_B) to produce and sustain an ITB with a fraction of bootstrap for a steady-state scenario $f_B \geq 50\%$: q_{95}=4-5, $\beta_N \geq 2$, ρ^*~5-6.
2. Optimisation of the hybrid advanced regime with electron heating to i) achieve an advanced regime of the hybrid type with dominant electron heating in stationary conditions; ii) investigate transport properties of optimised hybrid discharges; iii) prepare the development of hybrid scenarios with high β_N and low ρ^*.
3. Burning plasma.
4. Diagnostics experiments for i) characterisation of edge plasma; ii) measurements of oblique ECE; iii) validation of polarimetry data; iv) neutronics; v) assessment of accuracy of q-profile determination by motional Stark effect and vi) real-time control.

Comparison between the number of the proposals presented by ENEA, the United Kingdom Atomic Energy Authority (UKAEA), the Max-Planck Institute for Plasma Physics (IPP) and Forschungszeuntrum Jülich (FZJ) divided per task force (fig. 1.38) shows that the ENEA Association has presented proposals mainly for TF S2 (~30% out of a total of 42), D (~30% out of a total of 43) and M (~15% out of a total of 65).

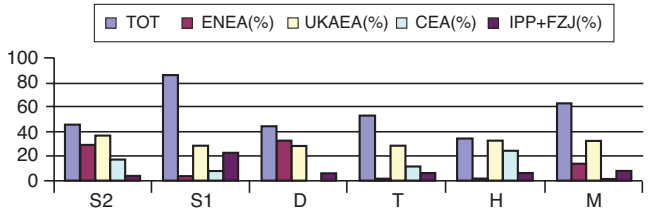

Fig. 1.38 - Number of proposals per task force presented by some European Associations

References

[1.69] P.U. Lamalle et al., *Investigation of low concentration tritium ICRF heating on JET*, presented at the 31st Eur. Physics Society Conf. on Plasma Physics (London 2004)

[1.70] V. Yavorskij et al., *Current hole effect on tritium beam in JET*, presented at the 31st Eur. Physics Society Conf. on Plasma Physics (London 2004)

[1.71] V. Kiptily et al., Phys. Rev. Lett. **11**, 115001 (2004)

[1.72] V. Kiptily et al., *Gamma-ray imaging of D and ^{4}He ions accelerated by ion-cyclotron-resonance heating in JET plasmas*, to appear in Nucl. Fusion

[1.73] B. Esposito et al., *Design analysis of ITER neutron camera diagnostic systems*, ENEA Internal Report FUS TN PHY-R-003 (December 2004)

[1.74] A. Zimbal et al., Rev. Sci. Instrum. **75**, 3553 (2004)

[1.75] B. Esposito et al., Rev. Sci. Instrum. **75**, 3550 (2004)

[1.76] L. Bertalot et al., *Fast digitizing techniques applied to scintillation detectors*, presented at the 9th Topical Seminar on Innovative Particle and Radiation Detectors (Siena 2004), to appear in Nuclear Physics B